

# Tectonics

## RESEARCH ARTICLE

10.1029/2018TC005177

### Special Section:

Collisional orogenic systems as recorders of collisions between arc and continents

### Key Points:

- The Wandamen Peninsula in West Papua consists of multiply deformed medium-high grade metamorphic rocks
- These rocks record multiple deformation events that occurred within the last six million years
- These rapid rates of deformation, metamorphism, and uplift should be considered in studies of ancient orogens and within numerical models

### Supporting Information:

- Supporting Information S1
- Data Set S1
- Data Set S2
- Data Set S3
- Data Set S4
- Data Set S5

### Correspondence to:

L. T. White,  
lloydw@uow.edu.au

### Citation:



White, L. T., Hall, R., Gunawan, I., & Kohn, B. (2019). Tectonic mode switches recorded at the northern edge of the Australian Plate during the Pliocene and Pleistocene. *Tectonics*, 38. <https://doi.org/10.1029/2018TC005177>

Received 7 JUN 2018

Accepted 12 DEC 2018

Accepted article online 19 DEC 2018

## Tectonic Mode Switches Recorded at the Northern Edge of the Australian Plate During the Pliocene and Pleistocene

L. T. White<sup>1,2</sup> , R. Hall<sup>2</sup> , I. Gunawan<sup>3</sup> , and B. Kohn<sup>4</sup> 

<sup>1</sup>GeoQuEST Research Centre, School of Earth, Atmospheric and Life Sciences, University of Wollongong, Wollongong, New South Wales, Australia, <sup>2</sup>Southeast Asia Research Group, Department of Earth Sciences, Royal Holloway University of London, Egham, UK, <sup>3</sup>Institut Teknologi Bandung, Bandung, Indonesia, <sup>4</sup>School of Earth Sciences, University of Melbourne, Melbourne, Victoria, Australia

**Abstract** We report new data from medium-high grade metamorphic rocks found at the northern margin of the Lengguru Fold Belt in West Papua. The study involved a systematic analysis of cross-cutting structures to establish the relative timing of deformation, together with isotopic dating to define when these tectono-thermal events occurred. These data show that the region underwent multiple episodes of deformation within the last six million years. Metamorphic mineral growth was associated with the development of ductile shear zones. This episode occurred during a phase of crustal stretching associated with the formation of a metamorphic core complex. Metamorphic zircon growth at 4.9 to 5.3 Ma was documented in two of the dated samples. These data are interpreted to postdate the peak pressure and temperature conditions of the phase of regional crustal stretching. The shear fabrics associated with the metamorphic core complex were later overprinted by at least two generations of folds. The change in mode from crustal extension to shortening reflects a tectonic mode switch. A subsequent mode switch is documented by numerous brittle extensional faults that cross-cut the earlier formed ductile fabrics. We interpret ca. 0.75–1.51 Ma (U–Th)/He age data to reflect cooling associated with the later stages of crustal shortening (marked by folds) or the later extensional unroofing of the peninsula. This work demonstrates that an orogen can record multiple tectonic mode switches within several million years. These outcomes should be considered in studies of ancient orogens where analytical uncertainties associated with isotopic dating may mask short-lived mode switches.

**Plain Language Summary** How much time is required for a mountain belt to develop? Our knowledge of mountain building is somewhat limited because many of the best-studied mountain belts are quite old and our ability to date tectonic events is less precise the farther back we look through time. The work presented here investigates a mountainous peninsula that developed at the northern margin of the Australian Plate within the last six million years. This region records multiple episodes of deformation—we show that the relatively young rocks have been stretched, then pushed together and then stretched again (much like an accordion). These cycles must occur over a period of one to two million years, which is very fast compared to numerous studies of ancient mountain belts that consider the same processes occur over tens of millions of years.

## 1. Introduction

Most of Earth's mountain belts form at plate boundaries—the rocks in these regions typically record multiple episodes of deformation that reflect the evolution of the ancient stress field where cycles of crustal shortening are overprinted by crustal extension (or vice versa; Balanyá et al., 1997; Beltrando et al., 2007; Collins, 2002; Forster & Lister, 2005; Froitzheim et al., 1994; Lister & Forster, 2009; Rawling & Lister, 1999). A change from crustal shortening to crustal extension (or vice versa) is known as a “tectonic mode switch” (Lister et al., 2001; Lister & Forster, 2009). Tectonic mode switches reportedly occur within <10 million-year periods (e.g., Beltrando et al., 2007, 2008; Dewey, 2005; Lister et al., 2001; Viete et al., 2013). In this paper, we examine a sequence of multiply deformed metamorphic rocks from the Wandamen Peninsula in western New Guinea (Figure 1). Previous work in this region indicates that these rocks were metamorphosed within the last 10 million years (Bladon, 1988; Francois et al., 2016). We suspect that these multiply deformed

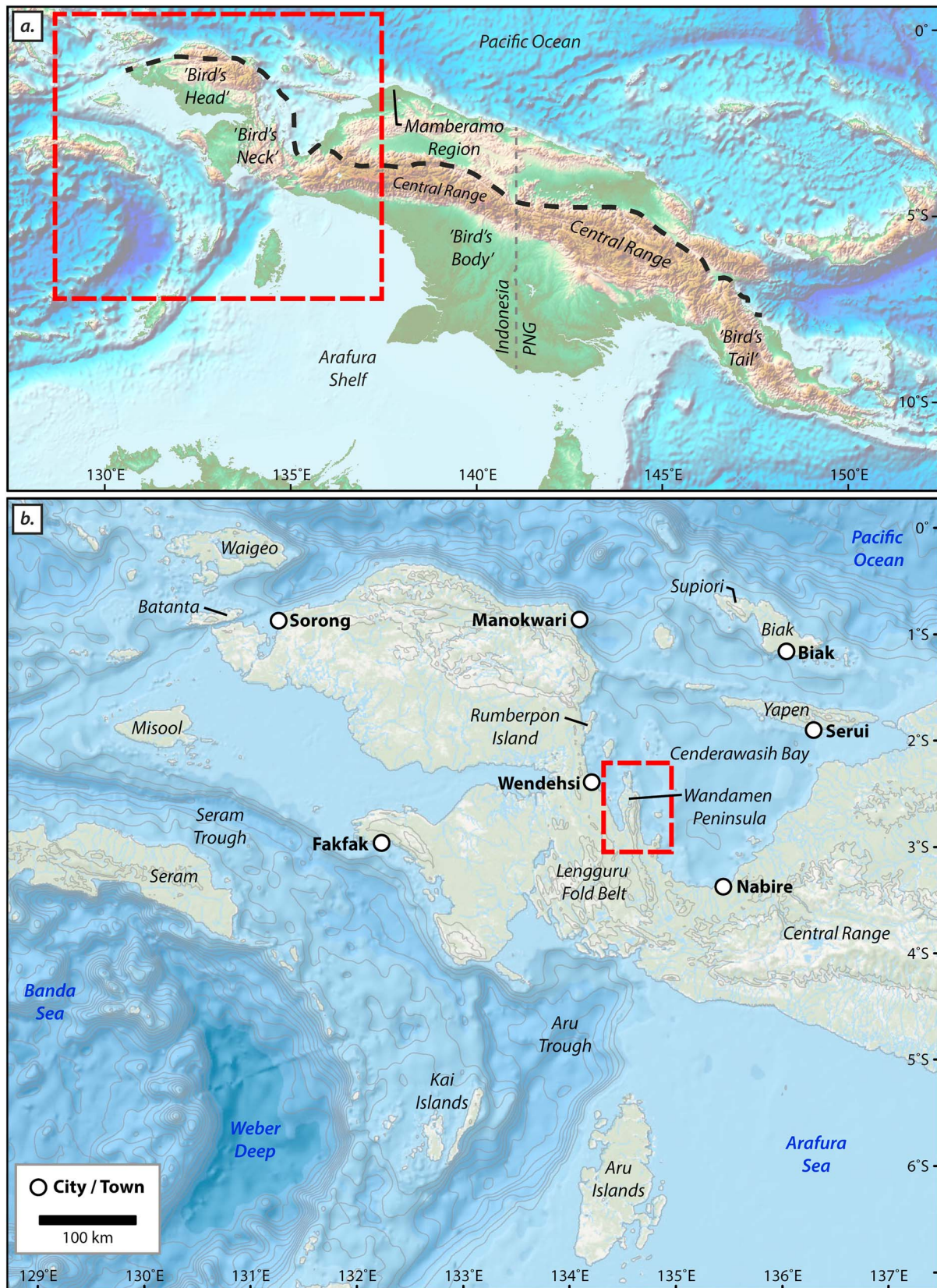


**Figure 1.** Maps showing the study area with reference to (a) New Guinea and (b) a larger scale map showing the location of the Wandamen Peninsula. Various geographic features and localities that are referred to in the text in both (a) and (b) are also shown.



metamorphic rocks potentially record information about the rates at which tectonic mode switches can occur on time scales of less than 10 million years.

Previous studies of the Wandamen Peninsula focused on the regional geology (Bailly et al., 2009; Dow et al., 1988) and metamorphic history (Bladon, 1988; Bailly et al., 2009; Francois et al., 2016). However, these studies report differences in the timing and sequence of deformation events. The timing of metamorphism is limited to several K/Ar ages (Bladon, 1988) and a few U-Pb ages of zircon (Francois et al., 2016; Figure 2). Francois et al. (2016) tentatively proposed two phases of metamorphic zircon crystallization at 8–7 and 6–5 Ma. However, these ages were based on dates obtained from several zircon grains obtained from one location on the northern coastline of the Wandamen Peninsula (Figure 2). It is possible that the 8–7 Ma zircon dates are not geologically meaningful, and instead reflect a mixed age from laser ablation-inductively coupled plasma-mass spectrometry (LA-ICP-MS) analyses of multiple growth zones within the zircon (i.e., partial analyses of inherited cores and younger metamorphic growth). It is important that these issues be resolved in order to understand the tectonic history of the region. We therefore systematically documented cross-cutting relations at different locations around the peninsula. These observations were taken from fresh exposures, oriented hand samples, and thin sections of metamorphic rocks to establish the sequence of deformation events. U-Pb age data were also collected from zircon extracted from nine samples to establish the timing of metamorphism and to characterize the protolith. We also collected (U-Th)/He data from zircon from three of the metamorphic rock samples to understand the timing of regional cooling relative to deformation phases.

## 2. Geologic Setting

North-western New Guinea currently marks a section of the boundary between the Australian, Caroline, and Pacific plates (Figure 1). A plate boundary has existed north of New Guinea since the Devonian where New Guinea represented the northern edge of eastern Gondwana (e.g., Baldwin et al., 2012; Davies, 2012; Gunawan et al., 2012; Jost et al., 2018; Webb & White, 2016). However, widespread deposition of carbonate sequences along the northern margin of New Guinea during the Cretaceous to early Eocene indicates that there was a period of relative tectonic quiescence on the southern (“Australian”) side of the plate boundary during this time (e.g., Gold, White, et al., 2017; Pieters et al., 1983; Visser & Hermes, 1962). Tectonic activity commenced once more in the mid–late Eocene with the final separation of the Australian and Antarctic plates at ~45 Ma (van den Ende et al., 2017; White et al., 2013) and subsequent rapid northward movement of Australian Plate (e.g., Schellart & Spakman, 2015; Schellart, 2017). This and later events are recorded through multiple episodes of magmatism, metamorphism, deformation, and uplift in New Guinea and eastern Indonesia (e.g., Ali & Hall, 1995; Bailly et al., 2009; Baldwin et al., 2012; Davies, 2012; Gold, White, et al., 2017; Pigram & Symonds, 1991; Sapin et al., 2009).

At least two major accretion events are recognized along the length of New Guinea between ~45 Ma and the present day; (1) the obduction of the Papuan Ophiolites, accretion of volcanic arc fragments of Pacific affinity, and the development of a widespread unconformity across western New Guinea and the southern Molucca's during the Oligo-Miocene (Ali & Hall, 1995; Gold, Burgess, et al., 2017; Gold, White, et al., 2017; Hall, 1996; Hall, Ali, & Anderson, 1995; Hall, Ali, Anderson, & Baker, 1995; Holm et al., 2013, 2015), and (2) accretion of the additional arc material during the Pliocene-Pleistocene (e.g., Davies, 2012; Dow et al., 1988; Holm et al., 2016; Monnier et al., 1999; Pigram & Symonds, 1991; Pubellier et al., 2003). These accretionary events are considered to have been driven by the northward advance of the Australian Plate since the Eocene and 40° clockwise rotation of the Philippine Sea Plate along the northern margin of the Australian Plate between the Early Neogene and present day (Ali & Hall, 1995; Hall, 1996, 2002; Hall, Ali, & Anderson, 1995; Hall, Ali, Anderson, & Baker, 1995; Hill & Hall, 2003). The deformation associated with these accretionary and other tectonic events ultimately produced New Guinea's unique topography—that is, an island that broadly represents a bird in flight—with the Bird's Head Peninsula found in the west, the Bird's Neck to the south/southeast, the central part of the island marking the bird's body, with its tail found at the eastern end of the island (Figure 1). The bird-like geometry is further defined by a mountain belt that extends through the Bird's Neck, Body, and Tail. This mountain belt is known as the Central Range in the Bird's Body and the Lengguru Fold Belt in the Bird's Neck (Figure 1). The work that is presented here focusses on the Wandamen Peninsula, considered here to be a component of the Lengguru Fold Belt (Moffat

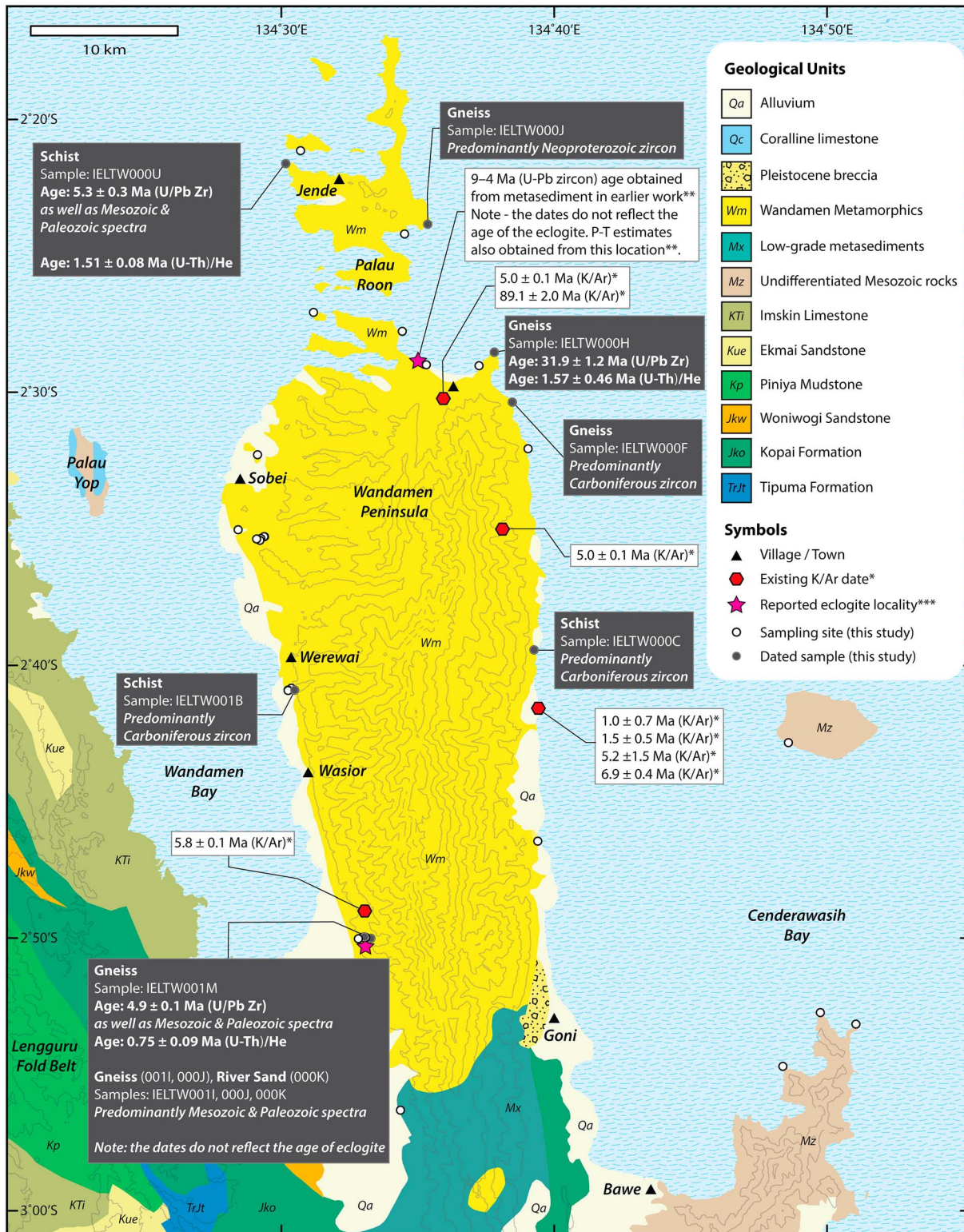


**Figure 2.** Map showing lithology and topography of the study area, together with the location and results of existing geochronological data and those obtained in this study. The maps also include the names of sampling/field localities as well as the sample numbers referenced to in the text, figures, and supplementary data. Readers interested in additional sample metadata are encouraged to read Data Set S1 and S2.



et al., 1991; Pieters et al., 1983; Visser & Hermes, 1962; Figure 1). The peninsula is essentially located between the Bird's Head Peninsula, the Bird's Neck, and the Bird's Body (Figure 1). There is some debate surrounding the relative movement of crustal fragments with respect to one another—particularly the direction, timing, and amount of rotation of the Bird's Head Peninsula (Charlton, 2010; Hall, 2012). This debate is not yet resolved, but the work that is presented here will add to a growing body of data that can be used to address such questions in the future.

### 2.1. The Lengguru Fold Belt

The Lengguru Fold Belt has an overall arcuate geometry that defines the shape of the Bird's Neck region (Figure 1). It consists of a series of anticlines and thrusts that deform the Cretaceous Simora Formation and Ekmai Sandstone, the carbonate sequences of the New Guinea Limestone Group (Late Cretaceous–Oligocene), and the marl and siltstone deposits of the Mio-Pliocene Klasafet Formation. The folded units are overlain by the various facies of the Plio-Pleistocene Steenkool Formation, some of which contain clasts of Eocene and Miocene carbonates. These rocks are age equivalent to the Klasaman Formation found in the Bird's Head and the Buru Formation found in the Central Range (Brash et al., 1991; Moffat et al., 1991).

The depositional and deformational history of the Lengguru Fold Belt is recorded in onshore exposures as well as in offshore seismic imagery. Field investigations show that at least two episodes of folding occurred at the Nabire/Weyland region at the eastern edge of the Lengguru Fold Belt (Dow & Ratman, 1981). The early phase consisted of isoclinal folds with steep axial planes, and these fabrics were overprinted by tight folds with subhorizontal fold axes. Aspects of this history are captured in offshore seismic imagery (Bailly et al., 2009; Sutriyono & Hill, 2001) (Figures 3a–3b). This imagery shows that the Klasafet Formation and older units are folded. This episode of folding occurred before or at the same time as the development of a regional Pliocene unconformity (Figure 3b). The earlier formed folds and unconformity were later cross-cut by Plio-Pleistocene extensional faults (Figure 3b). Parts of the region have also been cross-cut by relatively recent strike-slip faults, such as the <2 Ma Tarera-Aiduna fault zones (e.g., Pubellier & Ego, 2002).

While the deformation sequence is relatively clear, our ability to precisely date the timing of deformation events is currently limited to the biostratigraphic ages previously assigned to chronostratigraphic units. The level of precision is low because few publicly available biostratigraphic data exist and because the data available for Mio-Pliocene sequences above and below the unconformity contain microfossils that are not particularly age diagnostic. We tried to minimize this uncertainty, by revising the ages that were assigned to the Klasafet and Steenkool formations using planktonic foraminifera reported for each formation within the onshore 1:250,000 geological map sheets and the ASF-1X exploration well (Robinson, Harahap, et al., 1990; Robinson, Ryburn, Harahap, Tobing, Achdan, et al., 1990a; Robinson, Ryburn, Harahap, Tobing, Bladon, et al., 1990b) together with the most recent geological time scale (Gradstein et al., 2012; Figures 3a and 3c). Our revision of available biostratigraphic data shows that there is an approximately five million-year period of uncertainty in defining the chronostratigraphic boundary between the two sequences (i.e., between 11.5 and 5.5 Ma). We recognize that this interpretation is a crude and oversimplified attempt at biostratigraphic dating—but this reflects the limited data available for the region that exists in the public domain. The uncertainty associated with the age of these sedimentary sequences explains why some workers consider that folding of the Lengguru Fold Belt began at ca. 11 Ma (e.g., Bailly et al., 2009; Francois et al., 2016) while others propose folding occurred much later at ca. 5 Ma (Decker et al., 2009; Dow et al., 1985; Moffat et al., 1991; Pieters et al., 1983; Visser & Hermes, 1962).

The uncertainty that surrounds the timing of folding and uplift is also partly due to model-driven interpretations of the regional stratigraphy and tectonic history of the region. For instance, Bailly et al. (2009) considered deformation of the Klasafet Formation was synchronous with its deposition. However, it is equally plausible that these beds were deformed after their deposition. Other workers have interpreted the deposition of the Klasafet Formation to mark the initial stage of collision/accretion during the mid-to-late Miocene (Brash et al., 1991). Their rationale was that the deposition of deeper water sediments reflected rapid subsidence associated with flexure caused by arc-continent collision. This interpretation is possible, but is dependent on the location of sedimentation with respect to the plate boundary and the growing mountain belt. The opposite scenario is also plausible, that is, shallower conditions could develop due to surface uplift associated with deformation at the plate boundary. In fact, a change from marine to continental sedimentation in the suture zone between the Indian and Eurasian plates is one of the geological criteria used for

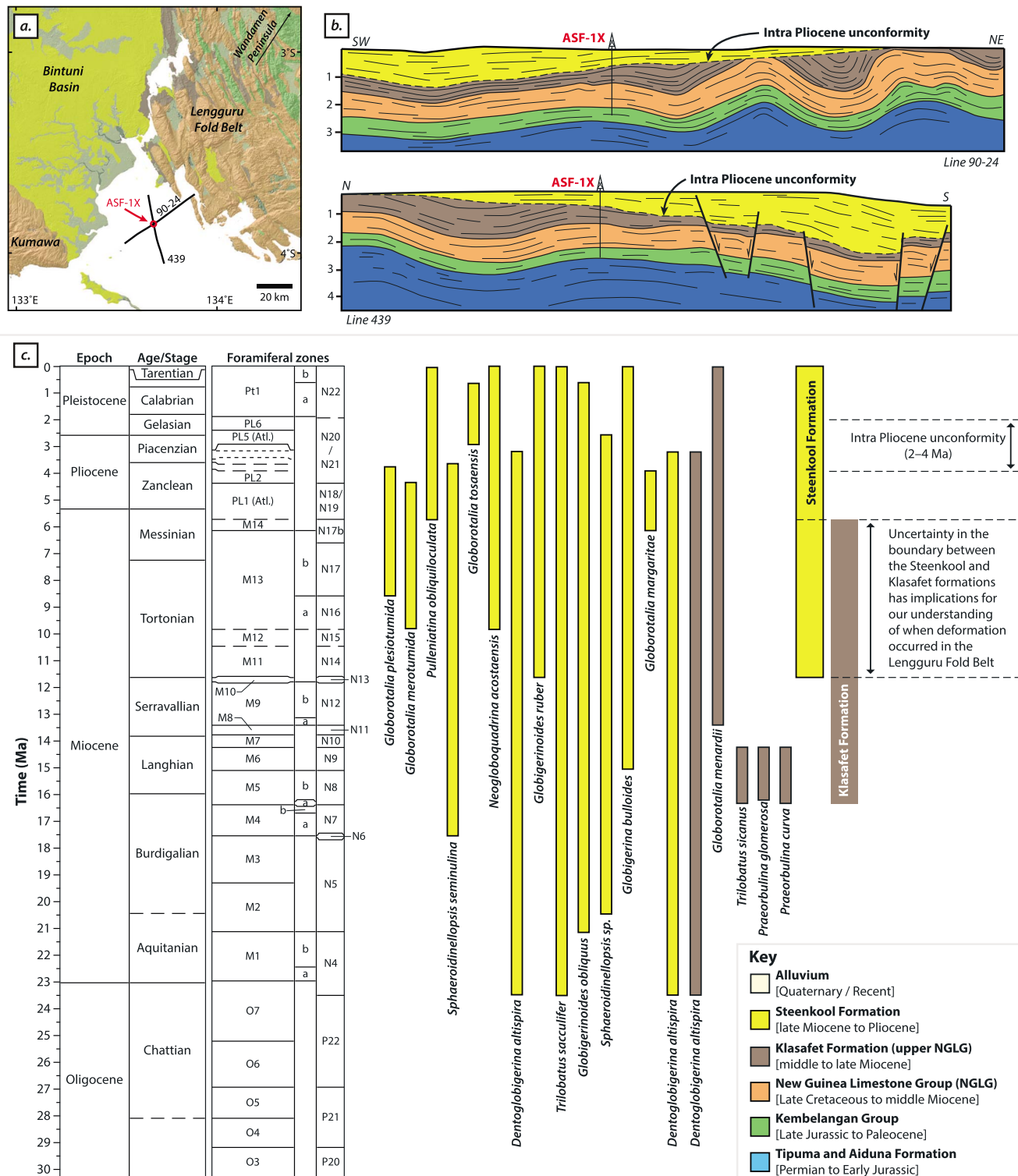


**Figure 3.** (a) Map showing the surface geology of the south-eastern Lengguru Fold Belt and Bintuni Basin, as well as the location of two seismic lines (Lines 90–24 and 43) and exploration well ASF-1X. (b) The geological interpretation of the seismic lines and corresponding well tie was adapted from Bailly et al. (2009). (c) Also shown is the age range of foraminifera obtained from the folded units beneath the intra-Pliocene unconformity (i.e., the Klasafet Formation): indicated on the interpreted seismic sections and the unfolded late Miocene to Pliocene sequences (i.e., the Steenkool Formation). The biostratigraphic data were obtained from existing 1:250,000 geological maps of the region (Robinson, Harahap, et al., 1990; Robinson, Ryburn, Harahap, Tobing, Achdan, et al., 1990a; Robinson, Ryburn, Harahap, Tobing, Bladon, et al., 1990b)— with age ranges having been updated according to the latest geological time scale (Gradstein et al., 2012) and age ranges reported on [www.mikrotax.org](http://www.mikrotax.org) (last accessed 8 April 2016).



define India-Eurasia collision (e.g., Aitchison et al., 2007; Searle et al., 1988). These issues simply highlight that more data are needed to test existing interpretations of the tectonic history of New Guinea.

## 2.2. The Wandamen Peninsula

The metamorphic rocks examined in this study were collected from the Wandamen Peninsula—a remote mountainous promontory at the northeastern margin of the Lengguru Fold Belt (Bailly et al., 2009; Dow et al., 1985; Visser & Hermes, 1962; Figures 1 and 2). The peninsula is approximately 70 km long and 18 km across, with some of the central parts being over 2,000 m above sea level (Figure 2). The peninsula is almost entirely composed of muscovite-biotite-quartzofeldspathic gneiss, biotite  $\pm$  garnet schist and amphibolite. Some exposures of metacarbonate as well as eclogite river detritus have also been reported (e.g., Figure 2 and supporting information Data Set S1). The metamorphic rocks are overlain by recently deposited alluvium dominated by angular metamorphic clasts (Dow et al., 1988; Dow & Ratman, 1981; Dow & Sukamto, 1984; Robinson, Ryburn, Harahap, Tobing, Achdan, et al., 1990a).

The metamorphic rocks are termed here the “Wandamen Metamorphics” (following Dow & Ratman, 1981; Dow & Sukamto, 1984), however, others have referred to these rocks as the “Wandamen Gneiss” (e.g., Bailly et al., 2009; Dow et al., 1988; Pieters et al., 1983; Robinson, Ryburn, Harahap, Tobing, Achdan, et al., 1990a). The metamorphosed quartzofeldspathic rocks mainly consist of quartz, plagioclase, K-feldspar, biotite, and muscovite, with rare porphyroblasts of garnet, epidote, and clinozoisite. These rocks have been considered to represent metamorphosed granitoids (Dow et al., 1988; Dow & Ratman, 1981; Dow & Sukamto, 1984; Robinson, Ryburn, Harahap, Tobing, Achdan, et al., 1990a). If true, the gneisses could represent granitoids found in the Bird’s Head and Cenderawasih Bay which range in age from Devonian to Triassic (see Bladon, 1988; Jost et al., 2018; Webb & White, 2016). The mineralogy of the schists is more variable (i.e., quartz + biotite  $\pm$  garnet  $\pm$  muscovite  $\pm$  kyanite  $\pm$  staurolite  $\pm$  sillimanite  $\pm$  tourmaline), with some exposures having garnets up to 10 cm in diameter (Francois et al., 2016). The mineralogy and geochemistry of the schists indicates they are predominantly metamorphosed sedimentary rocks, most likely from the Paleozoic Kemum Formation or Mesozoic Kembelengan Group found in the Bird’s Head and Neck, respectively (Bailly et al., 2009; Dow et al., 1988; Francois et al., 2016).

The earliest work on the Wandamen Metamorphics proposed that these rocks formed in the range of 520–730 °C and 5–9 kbar (Dow et al., 1988; Robinson, Ryburn, Harahap, Tobing, Achdan, et al., 1990a). Higher pressure estimates have been obtained from subsequent thermobarometric analyses of several samples from the northern and southwestern sections of the peninsula (Francois et al., 2016). Three metamorphic episodes have also been reported (Francois et al., 2016). These episodes include a prograde burial phase ( $M_1$ ) marked by garnet + kyanite + phengite schists that formed at medium–high pressure (12–16 kbar) and temperatures of >650 °C (Francois et al., 2016). A later lower pressure (10–12 kbar), but similar temperature (650–760 °C) phase ( $M_2$ ) was recorded from samples containing biotite and was interpreted to record later decompression (Francois et al., 2016). A final phase of metamorphism ( $M_3$ ) is recorded by late brittle fractures filled with chlorite, white mica, and quartz ( $P$ :  $6.8 \pm 1$  kbar and  $T$ :  $520 \pm 50$  °C; Francois et al., 2016). These temperature estimates are supported by those obtained from Raman carbon thermometry analyses of numerous samples across the peninsula (which record temperatures within the range of 330–660 °C; Bailly et al., 2009).

Less is known about the amphibolites and (retrogressed) eclogites found on the peninsula. These occur within metamorphic layers and as boudins within the schist and gneiss (Bailly et al., 2009; Dow et al., 1988; Francois et al., 2016). Fresh eclogite has so far only been recovered as river detritus (Bailly et al., 2009; Francois et al., 2016; Figure 2). Late Cretaceous high-pressure metamorphism was interpreted on the basis of an 89 Ma K-Ar age obtained from a piece of epidote amphibolite river detritus from the northern Wandamen Peninsula (Dow et al., 1988; Figure 2), but the rock that was dated was considered to represent a different lithology to the amphibolite boudins found within the Wandamen Metamorphics (Dow et al., 1988). Subsequent geochemical work indicates that the eclogites were likely derived from a primitive alkaline basalt, while the amphibolite was likely derived from a subalkaline tholeiitic series basalt or basaltic andesite typical of a volcanic arc—presumably derived from the Pacific Plate (Francois et al., 2016). Thermobarometry analyses indicate that the eclogite potentially reached pressures of 17–23 kbar and temperatures of 700–800 °C (Francois et al., 2016). These high-pressure rocks are not discussed in detail in this paper as they form the focus of another study.

Our knowledge of the approximate timing of metamorphism of the Wandamen Metamorphics is derived from K-Ar analyses of biotite, muscovite, and hornblende and U-Pb LA-ICP-MS analyses of zircon (Bladon, 1988; Dow & Ratman, 1981; Francois et al., 2016; Robinson, Ryburn, Harahap, Tobing, Achdan, et al., 1990a; Figure 2). The K-Ar analyses were collected from float samples and yielded ages between 7.3 and 0.3 Ma (Bladon, 1988; Dow & Ratman, 1981; Robinson, Ryburn, Harahap, Tobing, Achdan, et al., 1990a). Subsequent U-Pb dating of zircon yielded several ages between 9 and 4 Ma (Francois et al., 2016)—some of these analyses included dates of zircon with kyanite inclusions. The dates obtained from these zircon grains presumably reflect crystallization after  $M_1$  considering that metamorphic zircon growth typically postdates maximum pressure conditions (e.g., Kohn et al., 2015). Francois et al. (2016) speculated that the zircon age data they obtained recorded two episodes of zircon growth, one at 8–7 Ma and another at 6–5 Ma. However, these workers also considered that older age population may reflect a mixing age because the 9–7 Ma ages were obtained only from samples that recorded evidence of earlier zircon growth (i.e., inheritance recorded in zircon cores), while the 6–4 Ma ages were recorded in samples that showed no evidence of inheritance. One of our aims was to resolve this uncertainty by (1) analyzing samples collected from several locations across the Wandamen Peninsula (Figure 2); (2) analyzing ~50–100 zircons extracted from each sample (where possible), and (3) utilizing data reduction software that is capable of resolving the ablation of multiple age domains within zircon grains analyzed by LA-ICP-MS.

Our other major aim was to develop a more comprehensive understanding of the deformation history of the Wandamen Metamorphics. All previous workers recognize that the peninsula (1) contains antiforms with wavelengths of ~0.5–1.0 km, and (2) there is a dominant schistosity and pronounced north–south mineral or stretching lineation in some locations (Figure 4; e.g., Bailly et al., 2009; Dow et al., 1988; Dow & Ratman, 1981; Francois et al., 2016; Pieters et al., 1983; Robinson, Ryburn, Harahap, Tobing, Achdan, et al., 1990a). However, there has been little discussion of the development of these structures. To address this lack of detail, we systematically documented cross-cutting relations in the field, as well as in hand samples and thin sections. We then applied our findings to regional geological data to revise existing interpretations of the tectonic evolution of the Bird's Head of New Guinea.

### 3. Methodology

#### 3.1. Fieldwork

Fieldwork was conducted on the eastern and northern coast of the Wandamen Peninsula in 2013 and along the western coast in 2014 (Figures 2 and 4). Both field seasons focused on documenting cross-cutting relations and collecting samples for detailed microstructural analysis and geochronological work. The fieldwork undertaken during 2013 was entirely conducted using a speed boat launched from a larger vessel that served as a floating base camp. The speed boat was used to access the remote sections of the rugged eastern coastline and inlets along the northern coastline. Much of the eastern coastline is difficult to access—it is isolated, covered in dense tropical vegetation, and the terrain is very steep.

A subsequent field campaign was undertaken in 2014. This involved sampling road exposures and river traverses along the western coastline of the peninsula. Fresh exposures of rock are common and are relatively easy to access. However, access to the interior of the peninsula is more difficult due to the rugged terrain and dense tropical rainforest vegetation.

Each of the field sites indicated on Figure 2 represent locations where observations and samples were collected. A more detailed sample map and collection of photographs is provided in Data Set S2. Sample metadata (locations and descriptions) have been recorded using International GeoSample Numbers registered using the System for Earth Sample Registration (<http://www.geosamples.org/>). These data are also available provided in Data Set S1.

#### 3.2. Structural Analysis

Cross-cutting relations were documented using the sequence diagram approach (Beltrando et al., 2008; Forster & Lister, 2008; Viete et al., 2010). This method involves recording observations of cross-cutting relationships observed at exposures, followed by a compilation and comparison of the sequences seen in the region. Subsequent examination of microstructures and textures observed in hand specimens and thin sections can also be combined with the field evidence to build a comprehensive sequence diagram for a given



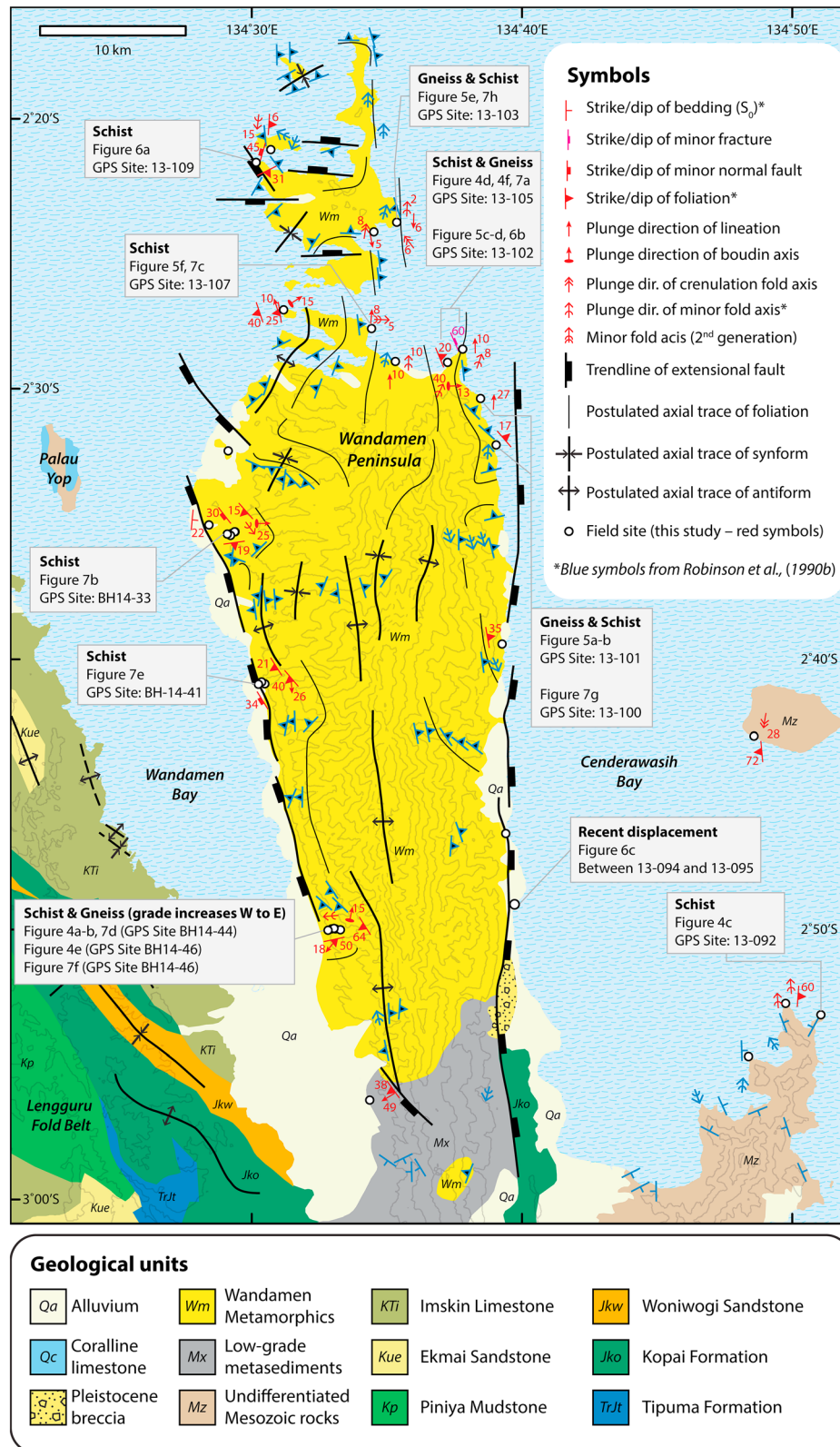


**Figure 4.** Map showing lithology, topography, and structure of the Wandamen Peninsula. This includes the structural data from Robinson, Ryburn, Harahap, Tobing, Achdan, et al. (1990a) indicated by blue symbols, as well as representative structural data collected from 28 coastal, river, and roadside outcrops during this study (red symbols). Structural observations were typically recorded across 10–20 m wide exposures. The location of photographs shown in subsequent figures have been indicated on this map.

**Table 1**

*TSDs Consist of Using a Series of Annotations to Describe the Sequence of Cross-Cutting Structures and Metamorphic Mineral Growth Events at an Outcrop and/or in a Sample*

| Annotation                     | Description                                                                                                                                  |
|--------------------------------|----------------------------------------------------------------------------------------------------------------------------------------------|
| S  SL                          | Bedding fabric (S0) with one or more parallel fabrics overprinting (difficult to differentiate between fabrics)                              |
| S                              | Fabric with unrelated folding event                                                                                                          |
| F                              | Folds                                                                                                                                        |
| F <sub>R</sub>                 | Recumbent folds                                                                                                                              |
| F <sub>R</sub> chevron         | Recumbent chevron folds                                                                                                                      |
| F <sub>U</sub>                 | Upright folds                                                                                                                                |
| SZ <sub>NE</sub>               | Shear zone with denoted lineation trend direction                                                                                            |
| FLT                            | Brittle fault                                                                                                                                |
| FLT <sub>EXT/REV/DEX/SIN</sub> | Brittle fault with EXT = extensional; REV = reverse; DEX = dextral; or SIN = sinistral sense of movement                                     |
| → → SZ → →                     | → → Above sequence: duration of shear zone activity                                                                                          |
| > > SC>>>>>>                   | >>>> > Below sequence: duration of specific event (e.g., S–C fabric)                                                                         |
| Δ (e.g., ΔBt)                  | Static metamorphic mineral growth event (e.g., biotite assemblage)                                                                           |
| Δ<br>Bt<br>>>>>                | Metamorphic mineral growth event (e.g., Bt) that continues for the specific duration marked by arrows below TSD                              |
| Δ<br>Bt<br>>>>>                | Metamorphic mineral growth event (e.g., Bt) that is initially static but then continues for the specific duration marked by arrows below TSD |

*Note.* The nomenclature is largely the same as that used by Forster and Lister (2008), however, several additional annotations were added to suit the particular region that was studied. TSD = tectonic sequence diagram.

locality. Sequence diagrams from different localities are then compiled and compared to decipher the broader deformation sequence of a region. Elements of a deformation sequence may not be recorded at every location due to differences in the mechanical properties of the rocks as well as the orientation of the local strain field. However, the sequence diagram approach accommodates these uncertainties and removes bias involved in assigning particular structures to the traditional numbered deformation events on the basis of style or orientation.

We used a form of shorthand, adapted from Forster and Lister (2008), to record the tectonic sequence diagrams (further explained in Table 1). All of these structural observations were documented on-site and were collected from fresh exposures. These sites were further characterized using observations made from oriented samples and oriented thin sections.

### 3.3. U-Pb and (U-Th)/He Geochronology

U-Pb geochronology data were collected from nine samples of schist and gneiss and one sample of modern river sand (Figure 2) to document the timing of metamorphic zircon growth and to examine the detrital age spectra of the metamorphic protolith. The samples were processed in the laboratories at Royal Holloway University of London. Rock samples were first pulverized using a jaw crusher. Aggregate <~1 cm<sup>3</sup> was discarded to minimize the risk of residual contaminants within the jaw crusher. All material >1 cm<sup>3</sup> was washed and dried before being milled using a Fritsch Pulverisette 13 tungsten-carbide disk mill. The milled aggregate and river sand were dry-sieved to obtain material <250 μm before each sample was washed once more—the finest grain fractions were decanted and discarded. Heavy and light mineral separates were obtained from this material through the use of a Wilfley-Table, magnetic separation, and diiodomethane. Zircon from each sample was then hand-picked and set into epoxy resin along with the Temora II U-Pb



standard (Black et al., 2004). The polished mounts were photographed under transmitted and reflected light and imaged using a Hitachi S3000 Scanning Electron Microscope at Royal Holloway University of London to obtain secondary electron and cathodoluminescence images to document internal growth zones within each zircon.

U-Pb isotopic ratios of targeted zircon grains were then collected using a New Wave NWR 193 laser ablation system coupled to an Agilent 7700 quadrupole-based inductively coupled mass spectrometer (LA-ICP-MS) at the London Geochronology Centre, University College London. Plešovice zircon was used as the internal standard to age calibration (Sláma et al., 2008), while Temora II was treated as an unknown to assess the results obtained from each analytical session. NIST SRM 612 glass (Pearce et al., 1997) was used as a trace element standard for U and Th compositional data. The resultant data were reduced using Iolite v3.6 (cf. Paton et al., 2011), the U\_Pb\_GeochronologyX data reduction scheme (cf. Paton et al., 2010), and a  $^{235}\text{U}/^{238}\text{U}$  ratio of 137.818 (Hiess et al., 2012) and broadly follow the protocols defined by Horstwood et al. (2016). Data reduction involved integration of the baseline, standards, and unknowns for five analytical sessions (typically with the manual selection of 10–15 s integration periods). Shorter integrations were used for several analyses of unknown zircon where spectra (e.g., U, Th, La,  $^{235}\text{U}$ ) showed significant differences within an analysis. These cases were double-checked and were typically found to correspond to mixed spectra associated with ablation through multiple age growth zones—where an age was determined for the core or rim. Results that are <1 Ga are reported using the  $^{238}\text{U}/^{206}\text{Pb}$  system, while older ages are reported using the  $^{207}\text{Pb}/^{206}\text{Pb}$  system. A common-Pb correction was not applied. Weighted mean ages and relative probability plots were generated using IsoplotR (Vermeesch, 2018). Additional information is provided in Data Set S3.

Zircon separates for three samples that contained clear evidence of young metamorphic zircon growth were later sent to the University of Melbourne for (U-Th)/He analyses. Two of the samples were collected at 1–15 m above sea level (IELTW000H; IELTW000U), the other was collected at ~240 m above sea level (IELTW001M; Figure 2). Five zircons containing two crystal terminations were selected from each sample. The analyses were conducted following the methods of Gleadow et al. (2015), the only difference being that our samples were spiked with  $^{233}\text{U}$  and  $^{229}\text{Th}$ . Further, we utilized the Fish Canyon Tuff zircon reference material (e.g., Gleadow et al., 2015; Phillips et al., 2017) as an internal unknown as a further check during analysis.

## 4. Results

### 4.1. Structural Analysis

Measurements of the orientation of representative structures were collected at each field site. The structural data were plotted on a geological map—together with the structural data reported by Robinson, Ryburn, Harahap, Tobing, Achdan, et al. (1990a; Figure 4). Cross-cutting relations were recorded at each field site using the sequence diagram approach. These observations were combined with additional observations from hand specimens and thin sections. All of these data were compiled to generate a tectonic sequence diagram for each visited location which are summarized in Table 2. Representative photographs of the deformation sequence are shown in Figures 5–8. A more comprehensive record of cross-cutting relations observed at each field site, thin section, and hand sample are provided in Data Set S2.

The revised geological map demonstrates that the dominant schistosity shows considerable variation in strike and dip across the peninsula (Figure 4). The variable orientation of the dominant, early formed schistosity is because these fabrics were subsequently folded by at least two generations of folds (Figures 4, 5, Data Set S2, and Table 2). This reorientation caused the rotation of shear-sense indicators, means that these structures cannot be reliably used to infer crustal extension or shortening. However, the widespread presence of boudinaged layers (as well as the boudins containing amphibolite and retrogressed eclogite) demonstrate that the Wandamen Metamorphics underwent a phase of stretching. The boudinaged layers have been folded (Figure 5). We have therefore interpreted that the boudinaged layers developed due to layer parallel stretching before folding, either during the development of the regional, dominant schistosity, or at the same time as the development of C/C' shear fabrics (Table 2). However, it is also possible that boudinage occurred due to layer parallel stretching during the episode of folding—this uncertainty is recorded in the sequence diagrams shown in Table 2. The folded ductile shear fabrics were subsequently cut by brittle extensional

**Table 2**  
*Tabulated Sequences of Tectonic Events Determined by Structural Analysis From Field, Hand Sample and Thin Sections at Key Localities Around the Wandaman Peninsula*

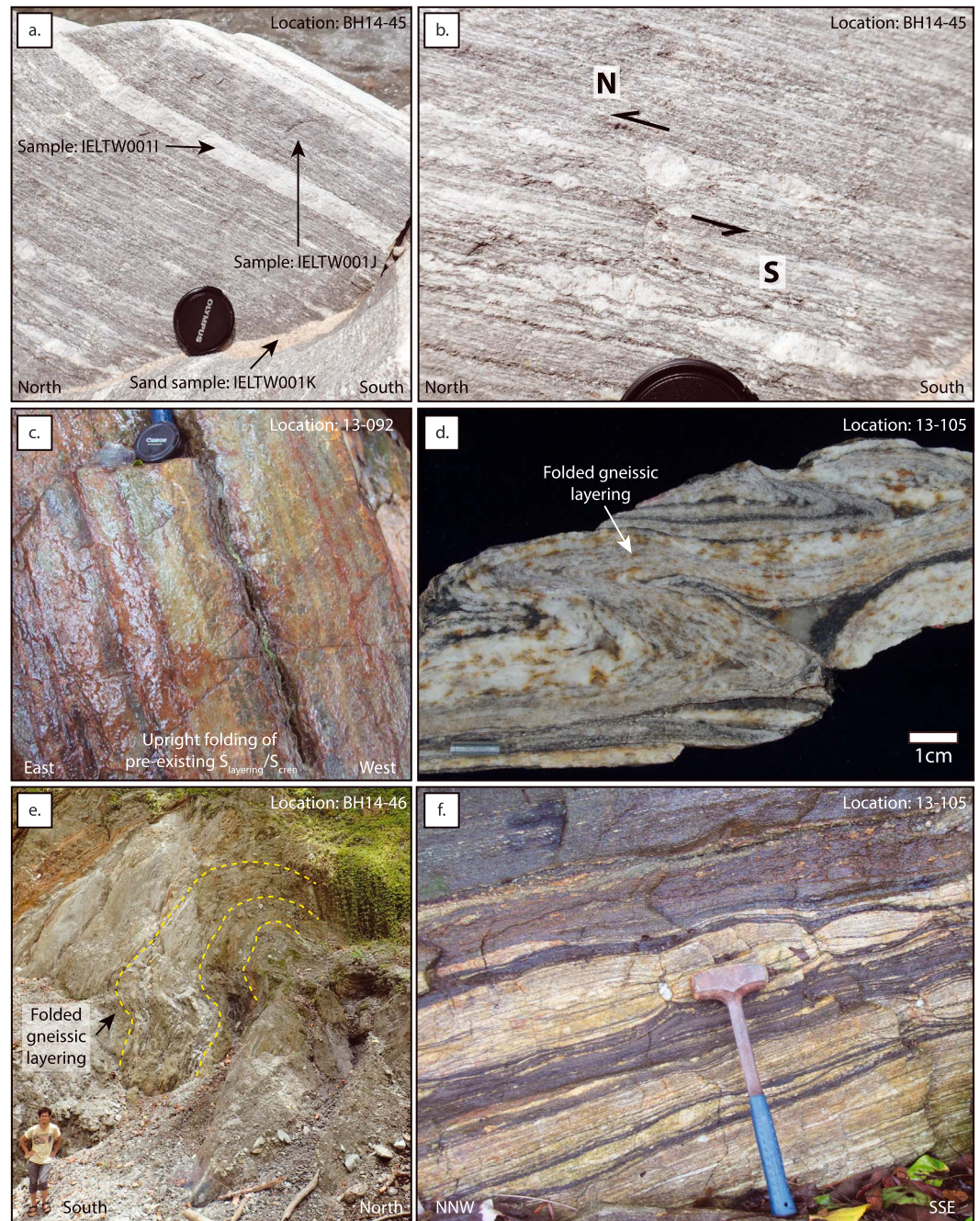
| GPS locality        |                                                         | Tectonic sequence diagram                         |                                                                                |                                        |                    |
|---------------------|---------------------------------------------------------|---------------------------------------------------|--------------------------------------------------------------------------------|----------------------------------------|--------------------|
| 13-091              | S  S <sub>L</sub>                                       | S <sub>Cren.</sub>                                | S <sub>Diff.</sub> Cren.<br>F <sub>U</sub>                                     |                                        |                    |
| 13-092              | S  S <sub>L</sub><br>ΔBt                                | S <sub>Cren.</sub><br>ΔBt<br>ΔTour                | F <sub>U</sub>                                                                 |                                        |                    |
| 13-093              | S  S <sub>L</sub><br>ΔBt/Musc                           | SZ<br>Interchangeable                             | F <sub>U</sub><br>Interchangeable                                              |                                        |                    |
| 13-094              | S  S <sub>L</sub>                                       | S <sub>Cren.</sub><br>ΔCalc<br>ΔTour              | S <sub>Diff.</sub> Cren.                                                       |                                        |                    |
| Between 094 and 095 |                                                         |                                                   |                                                                                |                                        | FLT <sub>EXT</sub> |
| 13-096              |                                                         | S <sub>Cren.</sub>                                | S <sub>Diff.</sub> Cren.                                                       | Erosion/deposition<br>of schist clasts |                    |
| 13-099              | S  S <sub>L</sub>                                       | SZ <sub>ENE</sub><br>>>>>>>>>>>>>>>               | F <sub>R</sub>                                                                 |                                        |                    |
| 13-100              | S  S <sub>L</sub><br>ΔMusc                              | SZ <sub>NNE</sub><br>>>>>>>>>>>>>>>               | F <sub>R</sub>                                                                 |                                        |                    |
| 13-101              | S  S <sub>L</sub><br>ΔBt                                |                                                   | F <sub>U</sub><br>Rodding(N-S stretching)                                      |                                        | FLT <sub>EXT</sub> |
| 13-102              | S  S <sub>L</sub>                                       | F <sub>R</sub><br>S <sub>Cren.</sub>              | F <sub>U</sub><br>Rodding(N-S stretching)                                      |                                        | FLT <sub>EXT</sub> |
| 13-103              | S  S <sub>L</sub>                                       |                                                   | F <sub>U</sub><br>Rodding(N-S stretching)<br>S <sub>Cren.</sub> >>>>>>>>>>>>>> | S <sub>Diff.</sub> Cren.               | FLT <sub>EXT</sub> |
| 13-104              | S  S <sub>L</sub><br>ΔMusc./Gt<br>>>>>>>>>>>>>>>>>>>    | SZ <sub>S</sub>                                   | F                                                                              |                                        |                    |
| 13-105              | S  S <sub>L</sub><br>ΔBt                                | SZ <sub>N</sub>                                   | F <sub>R</sub>                                                                 |                                        |                    |
| 13-106              | S  S <sub>L</sub><br>ΔBt/Musc/Gnt<br>>>>>>>>>>>>>>>>>>> | SZ                                                | F <sub>R</sub>                                                                 |                                        |                    |
| 13-107              | S  S <sub>L</sub><br>ΔBt/Musc./Gnt.                     | SZ                                                | F <sub>R</sub>                                                                 | F <sub>U</sub>                         |                    |
| 13-108              | S  S <sub>L</sub><br>ΔBt/Musc./Gnt.<br>ΔQtz veins       | SZ<br>>>>>>>>>>>>>>>>>>><br>Boudinage>>>>>>>>>>>> | F <sub>R</sub> /S <sub>Cren.</sub><br><br>>>>                                  |                                        |                    |



Table 2 (continued)

| GPS locality | Tectonic sequence diagram                     |                                   |                                      |           |  |                                          |
|--------------|-----------------------------------------------|-----------------------------------|--------------------------------------|-----------|--|------------------------------------------|
| 13-109       | S  S <sub>L</sub><br>ΔBt./Musc./Gnt.          | SZ                                |                                      |           |  | FLT <sub>EXT</sub><br>FLT <sub>REV</sub> |
| 13-110       | S  S <sub>L</sub><br>ΔBt./Musc./Gnt.          |                                   | F <sub>U</sub><br>S <sub>Cren.</sub> |           |  | FLT <sub>EXT</sub>                       |
| BH14-33      | S  S <sub>L</sub><br>ΔBt./Musc./Gnt.          | SZ<br>Boudinage>>>>>              | F <sub>U</sub><br>S <sub>Cren.</sub> | >>>       |  |                                          |
| BH14-34      | S  S <sub>L</sub><br>ΔBt./Musc./Gnt.          |                                   | F <sub>U</sub>                       |           |  |                                          |
| BH14-39      | S  S <sub>L</sub><br>ΔQtz./Bt./Musc.          | S                                 | F <sub>U</sub>                       |           |  |                                          |
| BH14-40      | S  S <sub>L</sub><br>ΔBt./Musc.               | SZ                                |                                      |           |  | FLT                                      |
| BH14-41      | S  S <sub>L</sub><br>ΔQtz./Muscovite          | SZ                                | F <sub>U</sub><br>Kinking            |           |  |                                          |
| BH14-43      | S <sub>0</sub>                                | S                                 |                                      |           |  | FLT                                      |
| BH14-44      | S  S <sub>L</sub><br>ΔGnt./Px./Bt.            | SZ<br>Boudinage>>>>>              | F <sub>U</sub>                       | >>>       |  |                                          |
| BH14-45      | S  S <sub>L</sub><br>ΔGnt./Bt./Musc.          | SZ<br>Boudinage>>>>><br>Myrmekite |                                      | >>>       |  |                                          |
| BH14-46      | S  S <sub>L</sub><br>ΔGnt./Musc.              | SZ<br>Kinking>>>>>>>>>            | F <sub>U</sub>                       | >>>>>>>>> |  |                                          |
| BH14-47      | S  S <sub>L</sub><br>ΔQtz.<br>ΔGnt./Bt./Musc. | SZ<br>ΔQtz. <sub>(ribbons)</sub>  | F <sub>U</sub>                       |           |  | FLT                                      |

*Note.* Items at the same locality are stacked vertically if we were unable to determine the relative sequence. The transport direction of displacement has been reported for some elements, however, in the majority of cases, these structures have been rotated due to subsequent deformation. Bt = Biotite; Musc = Muscovite; Gnt = Garnet; Qtz = Quartz; Tour = Tourmaline. Additional photographic evidence for each sequence is provided in the Data Set S2.



**Figure 5.** Photographs of folded gneiss from various locations around the Wandamen Peninsula. (a)–(b) represent samples IELTW001F (lightest, leucocratic material) and IELTW001G (darker gray material) and in their present-day orientation indicate top to the north, sense of shear; (c)–(e) provide clear evidence that the gneissic layering has been deformed by various stages and amounts of folding at different scales; (f) provides evidence of boudinaged gneissic layers—these fabrics have also been folded.

faults (Figures 7a–7b). This late extensional phase may have continued to the present day. For example, there are sections of submerged forest along the eastern side of the peninsula that mark the location of a slip surface (Figure 7c). Historical satellite imagery shows that this ~5 km long tract of land was submerged between December 2002 and December 2003 (<https://vimeo.com/286463271>; supporting information S1). People from the region stated that a tsunami occurred near this location in 2002—we suspect the tsunami and submerged block are related. This feature could have been driven due to sediment loading and/or liquefaction caused by a nearby earthquake in 2002 or 2003 (see supporting information S1).



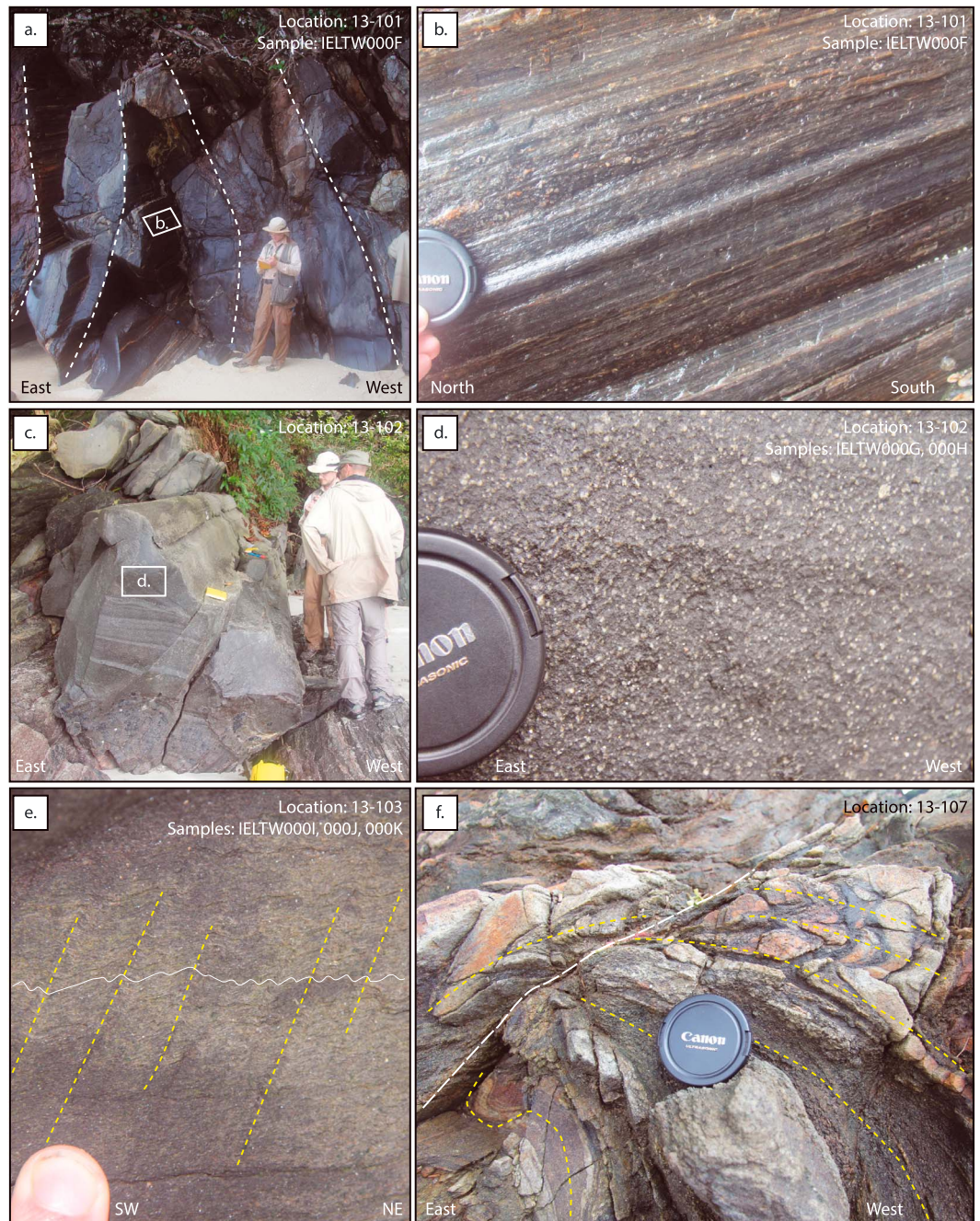


**Figure 6.** Photographs of (a–d) folds with a north–south axial plane as well as shallowly northward plunging plagioclase rods within the core of these folds. The earlier formed recumbent folds (e.g., Figure 4) are overprinted by a phase of (e) generally upright, differentiated crenulation cleavages and (f) open folds with a north–south trending axial plane.

#### 4.2. Petrography

The relative timing of metamorphic mineral growth can also be documented with respect to microstructures (and the overall tectonic sequence diagram; Table 2 and Figure 8). Biotite, muscovite, and garnet grew early during the deformation sequence—that is, at the same time as the regional schistosity ( $S_2$ ) that is subparallel to the metamorphic layering and original bedding. These fabrics were subsequently cross-cut by later shear fabrics. This relationship is demonstrated in numerous garnets, where porphyroblasts show evidence of rotation or boudinage (and many have been split in two; Figure 8). There is also evidence of two episodes of biotite growth—the earliest growth is associated with the development of the





**Figure 7.** All earlier fabrics are cross-cut by brittle extensional faults. This includes (a–b) mesoscopic structures that cross-cut schist and gneiss, as well as (c) apparent recent displacement of parts of the coastline into the sea.

regional schistosity ( $S_S$ ), the later growth is associated with the development of crenulations associated with the first generation of folds ( $F_R$ ; Table 2).

#### 4.3. Geochronology

U–Pb isotopic data were obtained from zircon extracted from nine samples of schist and gneiss as well as one stream sediment sample (IELTW001K; Figures 2 and 9, 10 and Data Sets S1, S3, and S4). Most of the samples yielded diverse age spectra interpreted to reflect detrital zircon from the metamorphic protolith (Figure 9). Carboniferous to Devonian ages are common in most of these schist, gneiss, and sediment samples (Data Set S4 and Figures 9b–9j). Some samples also record Triassic ages (Figures 9b–9c and 9j) and one sample of schist yielded primarily Proterozoic zircon (Figure 9d). Three samples yielded younger distinct age populations that could be interpreted to reflect metamorphic ages. One sample of quartz–biotite gneiss (IELTW000H) yielded a single age population, with a weighted mean age of  $31.9 \pm 1.2$  Ma (mean square weighted deviation (MSWD) = 0.6,  $N = 7$ ; Figures 9a and 10a)—this sample contained no older zircon. Two samples yielded Pliocene and older ages (Figures 2, 9b–9c, and 10b–10c)—this includes a quartz–biotite–garnet gneiss (IELTW001M) that yielded a weighted mean age of  $4.9 \pm 0.1$  Ma (MSWD = 1.0,  $N = 13$ ), and a quartz–muscovite–biotite schist (IELTW000U) that yielded a weighted mean age of  $5.3 \pm 0.3$  Ma (MSWD = 0.9,  $N = 9$ ; Figures 10b–10c).

Each sample contained zircon that differed in size and shape and had different internal textures (Figure 11). The Oligocene zircons extracted from IELTW000H (quartz–biotite gneiss) are strikingly different from all other samples (Figure 11g). These zircons are large oscillatory-zoned grains that yield Th/U values  $>0.1$  (Data Set S4) and show no evidence of earlier formed cores or younger rims. We therefore interpret this rock to be a paragneiss—with the zircon age reflecting the crystallization age of the protolith. The texture of the zircon could not be used to distinguish different age populations. These age populations were only resolved by obtaining the LA-ICP-MS data. For example, IELTW000J contained almost entirely Proterozoic zircon (Figure 9d). These zircon grains show evidence of igneous and metamorphic textures, as well as rims that grew around earlier formed cores (Figure 11a). Similar textures were obtained from most of the other samples, yet these zircon rims reflected Carboniferous growth. The Pliocene zircon grains were often obtained from oscillatory-zoned zircon grains with no inherited cores (e.g., Figure 11f)—yet these zircons all record Th/U values  $<0.1$  (Data Set S4) and we interpret these ages (4.9–5.3 Ma) to represent the timing of regional metamorphism.

#### 4.4. (U–Th)/He Thermochronology

(U–Th)/He dates were obtained from zircon separates from the three samples that yielded Oligocene and Pliocene zircon ages (IELTW000H; IELTW000U; IELTW001M; (Data Set S5). A weighted mean age was calculated for each sample:  $1.57 \pm 0.46$  Ma ( $n = 5$ ) [IELTW000H];  $1.51 \pm 0.08$  Ma ( $n = 5$ ) [IELTW000U];  $0.75 \pm 0.09$  Ma ( $n = 5$ ) [IELTW001M]. These results indicate that the samples that were collected at the northern end of the Wandamen Peninsula cooled through 180–200 °C at  $\sim 1.5$  Ma, while the sample from the southern part of the peninsula cooled through this range at 0.75 Ma (Figure 2).



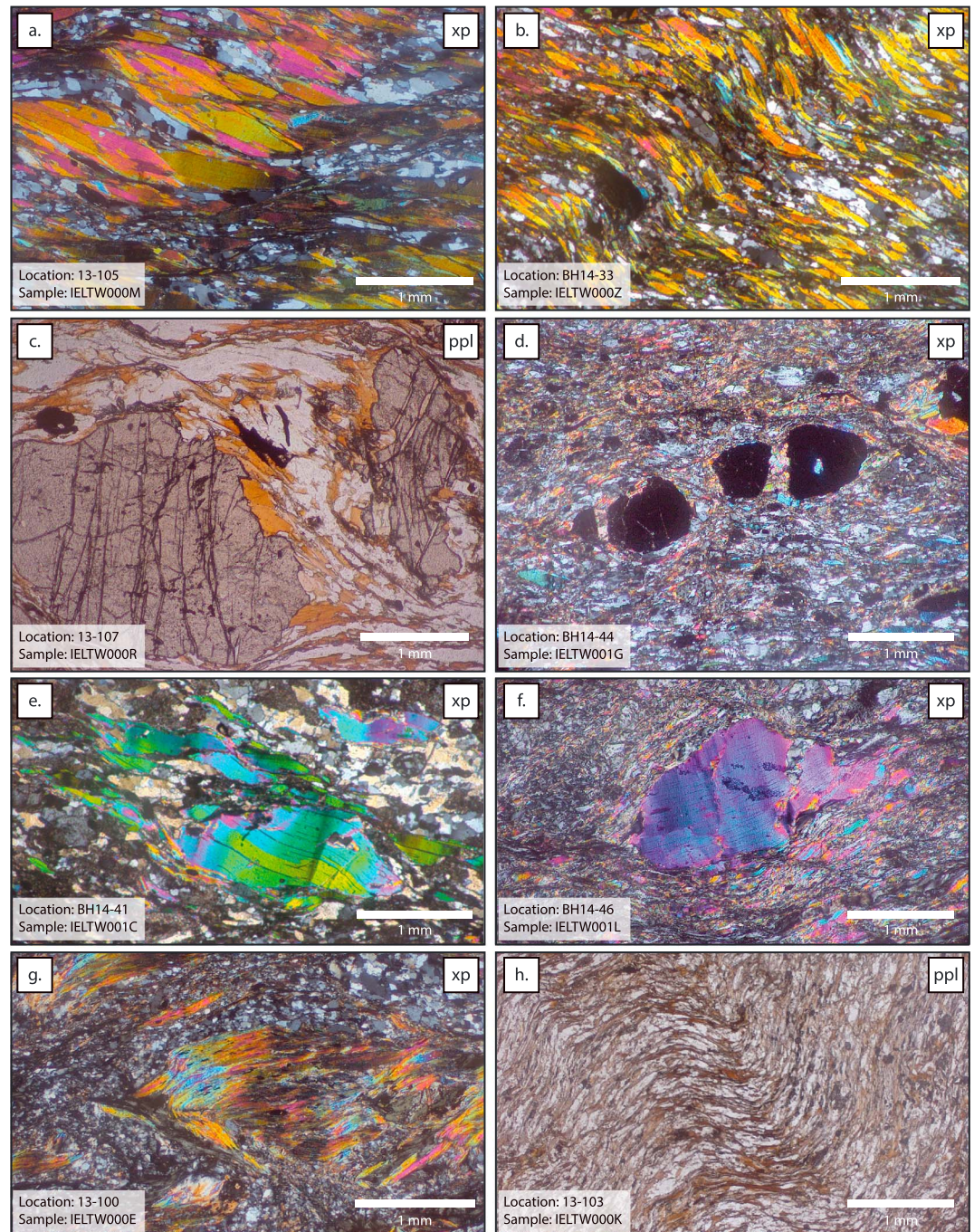


**Figure 8.** The same sequences of events that are observed in field and hand samples can be seen in thin sections. This includes (a–b) shear fabrics delineated with biotite and muscovite. (c–d) Garnet that grew early during the sequence (i.e., “M<sub>1</sub>”) has since been cut by extensional fabrics and boudinaged due to continued stretching; (e–h) shear fabrics delineated by earlier mica growth that have been kinked and folded.

## 5. Discussion

### 5.1. Differences Between our Results and Earlier Work

Our observations of cross-cutting relations indicate that there is a relatively consistent sequence of deformation events recorded across the Wandamen Peninsula (Figures 5–8, Table 2, and Data Set S2). These results conform to the relative sequence of deformation events recorded in offshore seismic imagery (e.g., Figure 3).

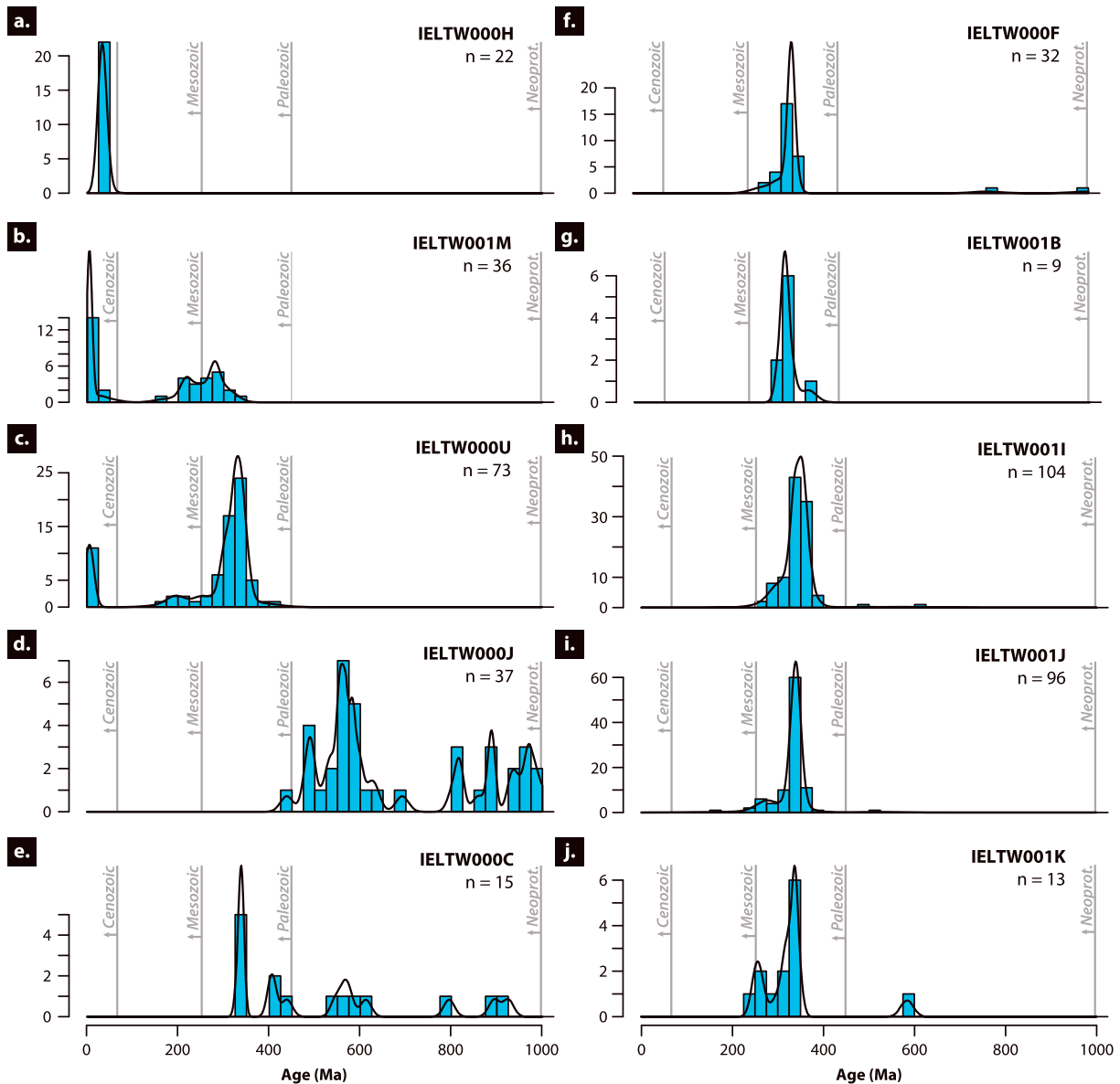


**Figure 9.** U-Pb age spectra of zircon from various (a–i) metamorphic rocks and (j) river sediment from the Wandamen Peninsula.

However, our results show some differences with earlier structural interpretations (e.g., Bailly et al., 2009; Francois et al., 2016). For instance, Francois et al. (2016) report that an early episode of folding was associated with the development of an axial planar “ $S_1$ ” fabric and these fabrics were cross-cut by S/C structures. We found no evidence of this deformation sequence. The earliest recognizable fabrics consist of a regional schistosity that is subparallel to bedding/layering. This regional schistosity was subsequently sheared (C/C’ planes) and folded within isoclinal, recumbent, and open folds (Figures 4–6, Table 2, and Data Set S2). Francois et al. (2016) also state that the shear fabrics (C/C’ planes) are associated with a north–south oriented stretching lineation which always indicates a top to the north sense of shear. We did not observe this relationship either. In the northern Wandamen Peninsula (where Francois et al., 2016, focused) the sense of shear obtained from S/C/C’ fabrics is approximately perpendicular to the pervasive north–south mineral or stretching lineation. The pervasive north–south stretching lineations occur in the core of later developed antiforms (Figure 5 and Data Set S2), and the earlier developed S/C/C’ fabrics have been rotated in the limbs of these folds (Figure 5 and Data Set S2). These rocks have fabrics that can be used to determine the sense of shear—but these structures have been overprinted and rotated by later



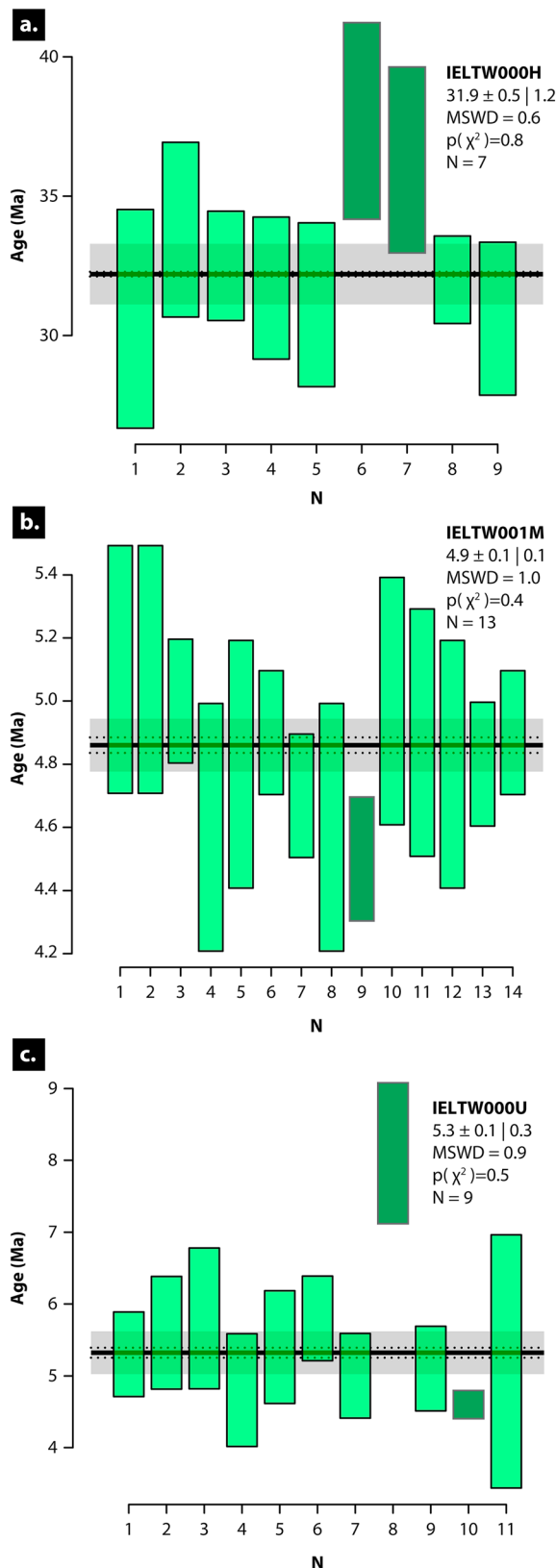


**Figure 10.** Weighted mean ages calculated for discrete age populations identified in samples (a) IELTW000H, (b) IELTW001M, and (c) IELTW000U.

folding, explaining why there is considerable variation of shear sense obtained across the peninsula (e.g., Figure 4).

Our observations of the deformation sequence differ to the sequence suggested by Francois et al. (2016)—primarily the earlier part of the deformation sequence. Despite these differences, our interpretation of the deformation sequence remains faithful to the relative timing of metamorphic mineral growth proposed by Francois et al. (2016). We therefore adopted the nomenclature Francois et al. (2016) used to identify metamorphic episodes ( $M_1$ ,  $M_2$ ,  $M_3$ ), as well as their thermobarometry data. A discussion of these metamorphic events ( $M_1$ ,  $M_2$ ,  $M_3$ ) relative to our structural observations and geochronology data is presented in the following section as well as in Figures 12 and 13.

## 5.2. Deformation Sequence

There is widespread evidence of an early schistosity that developed parallel to metamorphic layering and original bedding planes (e.g., Figure 5c and Data Set S2)—these fabrics were recognized by some of the earlier work in the region (e.g., Pieters et al., 1983), but not by others (e.g., Bailly et al., 2009; Francois et al., 2016). The 31.9 Ma age obtained from a quartz-biotite gneiss (IELTW000H) at the northern margin of the Wandamen Peninsula (Figures 2 and 10) is interpreted to reflect the emplacement of a granitoid in northern New Guinea. We assume this rock was deformed after it crystallized and it therefore may provide an upper bound to the deformation sequence (Table 2). However, we cannot determine if the protolith was originally emplaced within the northern Wandamen Peninsula, or if it was later transported via faults/shear zones. We have therefore related our structural and geochronological results to the existing petrological and thermobarometric data (e.g., Francois et al., 2016).

Pseudosections generated by Francois et al. (2016) indicate that the Wandamen Metamorphics were found at depths of ~45–60 km (12–16 kbar) and temperatures of >650 °C during  $M_1$  (Figure 12a). The regional schistosity and  $M_1$  garnets were later overprinted by shear fabrics (C and C'; e.g., Figures 5b and 8c–8d). These shear fabrics likely developed during a phase of crustal extension (Figure 13a)—explained by the shear fabrics and widespread occurrence of boudins that were subsequently folded. The ~5 Ma zircon ages are interpreted to reflect the cooling path of  $M_1$ —this interpretation factors in the zircon inclusions found within kyanite grains (e.g., Francois et al., 2016) and that metamorphic zircon crystallization records growth after peak P–T conditions (e.g., Kohn et al., 2015). Considering the structural and metamorphic evidence, we interpret the muscovite ± biotite ± garnet ± kyanite mineral growth to reflect part of a Barrovian sequence that developed as part of a metamorphic core complex due to crustal extension/transension at ~7–5 Ma (Figures 12c and 13a). This led to the development of a regional schistosity ( $S_S$ ), boudins, and partial melts, which were later cut by extensional shear zones that developed due to continued stretching (Figure 13a).

The ductile fabrics were overprinted by pervasive, predominantly N–S oriented stretching and mineral lineations (including rodding of feldspar at several locations; Figures 6b–6d). These lineations developed parallel to fold axes—similar to those studied in other parts of the world (e.g., Ridley, 1986). We propose that the stretching/mineral lineations developed at the same time as regional isoclinal folding (Figures 6a–6d and 13b). Such features can develop during transpression or pure shear of

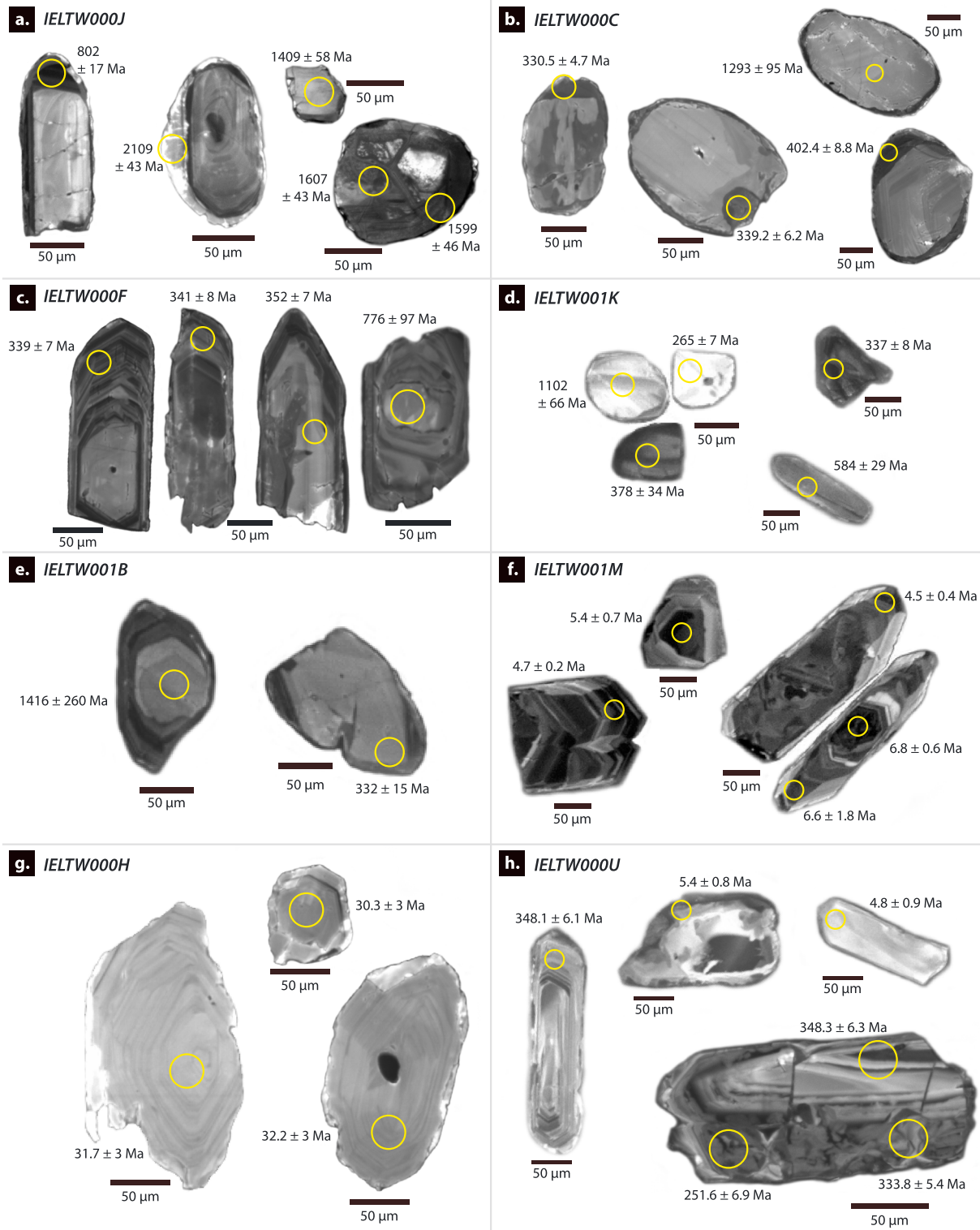


**Figure 11.** Representative scanning electron microscope cathodoluminescence imagery of zircon from samples (a) IELTW000J, (b) IELTW000C, (c) IELTW000F, (d) IELTW001K, (e) IELTW001B, (f) IELTW001M, (g) IELTW000H, and (h) IELTW000U. The location and result of individual laser ablation-inductively coupled plasma-mass spectrometry analyses are also shown.

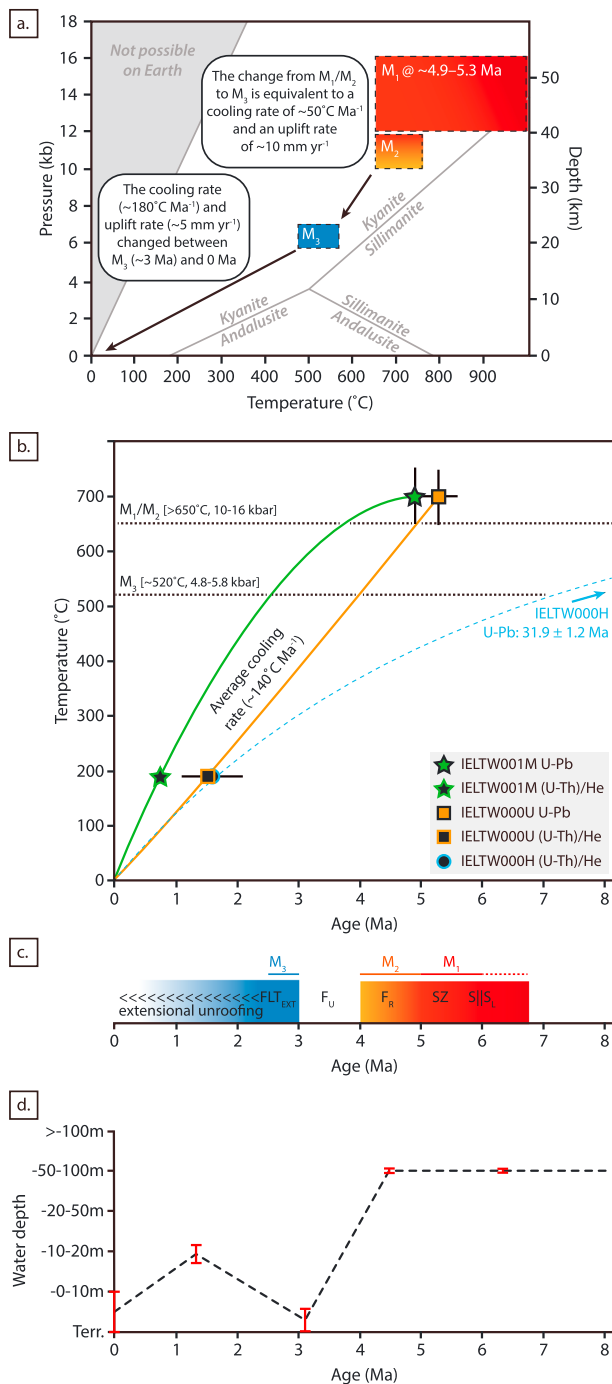


**Figure 12.** (a) Summary of thermobarometric results obtained for the Wandamen Metamorphics from the northern Wandamen Peninsula as reported by Francois et al. (2016). (b) U-Pb and (U-Th)/He age and approximate temperature estimates for metamorphic zircons from samples IELTW001M, IELTW000U, and IELTW000H. This plot also indicates an approximate cooling curve approximate temperatures estimated for each metamorphic phase ( $M_1$ ,  $M_2$ , and  $M_3$ —as reported by Francois et al., 2016). (c) Summary and interpretation of the age, structural, and thermobarometry data for the Wandamen Metamorphics. These data are comparable to (d) the record of fluctuations in regional (but not global) sea levels (modified from Gold, White, et al., 2017).

vertical/subvertical layers (e.g., Fossen et al., 1994; Fossen & Tikoff, 1998; Froitzheim, 1992). These features indicate there was a change in the stress field—we assume this change reflects a shift from predominantly east–west extension to contemporaneous east–west shortening and north–south stretching (using the modern-day orientation of fabrics). Continued shortening led to the development of recumbent folds in parts of the peninsula (Figures 4d and 5f) as well as north–south stretching (Figure 13b). A second phase of biotite growth ( $M_2$ ) occurred during the development of the early folds, with metamorphism occurring at pressures of 10–12 kbar and temperatures of 650–760 °C (Francois et al., 2016; (Figures 12a–12c and 13). These fabrics were subsequently deformed by open upright folds (Figures 5f and 13c) bringing the rocks to depths of 35–45 km (Figure 12a). We consider that the ductile  $M_2$  fabrics developed between  $\sim 5$  and  $\sim 4$  Ma—that is immediately after those that formed during  $M_1$  (Figures 12a–12c and 13b).

All of the fabrics were then cut by brittle extensional faults (with some minor associated thrust faults). It is these faults that contain the chlorite, white mica, and quartz growth that Francois et al. (2016) identified as  $M_3$  ( $P: 6.8 \pm 1\text{ kbar}$  and  $T: 520 \pm 50^\circ\text{C}$ ). These structures reflect a relative change in temperature and/or strain rate compared to the earlier developed ductile fabrics. We suspect this was due to rapid uplift of the metamorphic rocks from  $\sim 35\text{--}45$  to  $\sim 20$  km between  $M_2$  and  $M_3$  (Figures 12a–12c and 13c). The brittle extensional faults must have initiated at some point before  $\sim 1.5$  Ma if we consider the thermobarometry data of  $M_3$  together with the zircon (U-Th)/He data (with locking temperatures of  $\sim 180\text{--}200^\circ\text{C}$ ; Figures 12a–12c and 13d). The final phase of uplift must have consisted of  $\sim 20$  km of extensional exhumation between  $\sim 3$  Ma and the present day ( $\sim 5\text{ mm/year}$ ). This episode of tectonism is apparently continuing today—one example includes the  $\sim 5\text{ km}^2$  area of forest that subsided into the sea along the eastern edge of the Wandamen Peninsula between December 2002 and December 2003 (Figure 7c and supporting information 7S1; <https://vimeo.com/286463271>).

The difference in the two (U-Th)/He age populations likely reflects progressive north to south cooling and uplift of the peninsula (Figures 2 and 12b). We can calculate a cooling rate of  $\sim 140^\circ\text{C/Ma}$  if we assume that exhumation was linear between 5 and 0 Ma (Figure 12b). However, several episodes of stretching and shortening occurred during this time, so we suggest the cooling and uplift rates are better defined using the P-T estimates of Francois et al. (2016) combined with our geochronological results. These data indicate that the rocks cooled at a rate of  $\sim 50^\circ\text{C/Ma}$  and were uplifted at a rate of 10 mm/year between 7 and 3 Ma. The cooling rate later increased to  $180^\circ\text{C/Ma}$ , while the uplift rate decreased to  $\sim 5\text{ mm/year}$  between 3 and 0 Ma (Figure 12a). These rates are similar to those reported for other young metamorphic rocks found in Sulawesi (e.g., Hennig et al., 2017) and conform to the rates applied in numerical modeling of gneiss dome exhumation (e.g., Korchinski et al., 2018; Rey et al., 2017).

### 5.3. Evidence of Late Miocene Metamorphism

One of the aims of this study was to investigate evidence of 8–7 Ma metamorphic zircon growth reported by Francois et al. (2016). These 8–7 Ma ages were obtained from 1 to 2 zircon grains in three samples collected



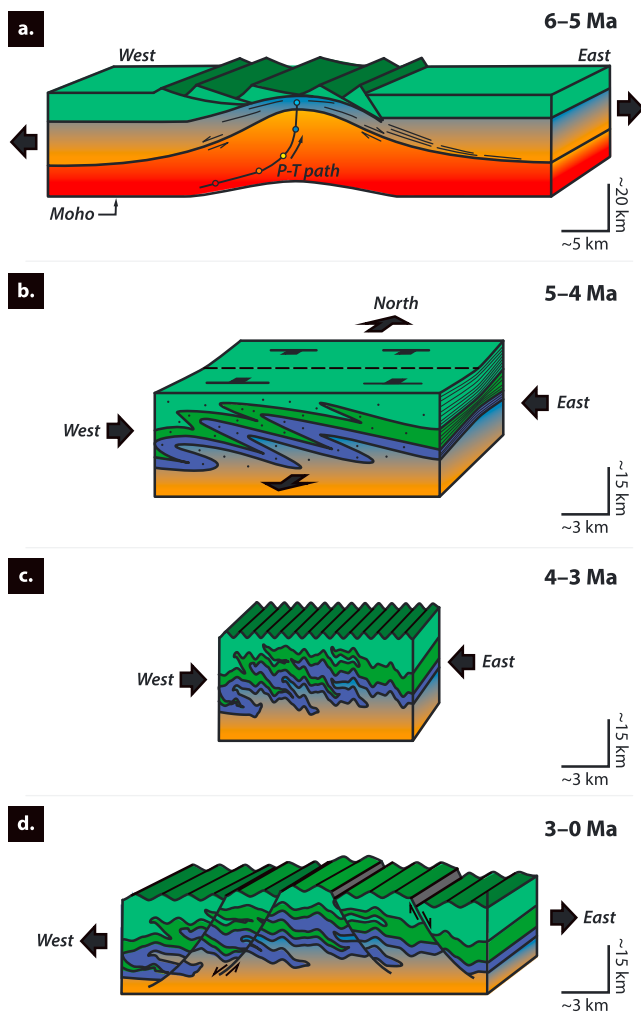


**Figure 13.** Schematic illustration showing the interpreted structural evolution of the Wandamen Peninsula/Wandamen Metamorphics using an approximate scale and orientations using the present-day orientation of the peninsula. (a) Crustal extension occurred during 6–5 Ma resulting in the development of a metamorphic core complex, bringing middle to lower crustal rocks closer to the surface quite rapidly. (b) The extensional fabrics were later recumbently folded (east–west shortening), with contemporaneous north–south extension producing rods/stretching lineations between 5 and 4 Ma. (c) A later phase of upright folding overprinted the earlier developed fabrics between 4 and 3 Ma. (d) All earlier fabrics were overprinted by brittle extensional faults and the peninsula was exhumed between 3 and 0 Ma. (a) was modified from Whitney et al. (2013).

different age spectra (IELTW000J and IELTW000H) from the other samples (Figure 9). These samples were collected on the northeastern edge of the Wandamen Peninsula and the island north of it (Palau Roon). The northernmost sample yielded almost entirely Neoproterozoic zircons (IELTW000J)—and was originally mapped as within an area of Devonian or older low-grade metamorphic rocks (Robinson, Ryburn, Harahap, Tobing, Achdan, et al., 1990a) with the age interpreted from field relations. This small area of Paleozoic or Neoproterozoic rock could represent a metamorphosed equivalent of the Kemum or Aisasjur Formation. The other sample (IELTW000H) yielded a tight cluster of Oligocene ages (weighted mean age of  $31.9 \pm 1.2$  Ma). We interpret this sample to represent a metamorphosed granitoid or felsic volcanic—its weighted mean age indicates this sample is potentially related to the Paleogene Arfak/Mandi Volcanics (e.g., Pieters et al., 1983) although these units consist of basalts and basaltic andesites. The sample dated in this study potentially represents a more felsic component of the Oligocene island arc that developed at

from one locality in the northern Wandamen Peninsula. We hypothesized that the 8–7 Ma ages potentially reflected a mixing age because the samples also yielded ~5 Ma as well as older inherited ages. To test this hypothesis, we examined more samples ( $n = 10$ ) from seven different locations around the peninsula (Figure 2). We also analyzed a greater number of zircons per sample ( $n = \sim > 50$  analyses, where Francois et al., 2016, reported anywhere between 3 and 13 analyses per sample). In addition, we used *Iolite* to examine and process the raw LA-ICP-MS spectra (which can be used to show if different isotopic ratios are obtained due to laser ablation of different age domains within a zircon). In doing this work, we found no clear evidence for zircon growth at 8–7 Ma. We therefore suggest that the earlier reported 8–7 Ma dates (Francois et al., 2016) reflect mixing ages associated with the ablation of younger ~5 Ma zircon rims and older cores. The 8–7 Ma ages should not be interpreted as geologically meaningful.

#### 5.4. Metamorphic Protolith

Zircon was dated from nine samples of metamorphic rock collected in situ (as well as one sample of river detritus). The samples were collected from seven localities across the Wandamen Peninsula (Figure 2). Only two of the samples recorded Pliocene ages (IELTW001M and IELTW000U). We assume that the other samples (1) did not reach temperatures and pressures suitable for generating new zircon grains or new rim growth on existing grains, and/or (2) metamorphic rims were too thin to observe/analyze. Despite this, the age spectra obtained from these samples yield data that provides further insight into the metamorphic protolith (Figure 9). Most of these samples contain Devonian to earliest Jurassic zircons (dominated by Devonian, Carboniferous, and Triassic zircon). These zircons are interpreted to have been derived from the erosion and transport of material sourced locally (e.g., Gunawan et al., 2012). Recent geochronology studies have dated Triassic igneous rocks to the south, east, and northwest of the Wandamen Peninsula (Decker et al., 2017; Jost et al., 2018). Evidence of Devonian-Carboniferous magmatism was also reported by Jost et al. (2018). These studies reported Paleozoic ages from outcrops in the Bird's Head, so the data we report here indicate that some of these Paleozoic igneous rocks may have been eroded and redeposited.

We take the youngest zircon from each of the Wandamen metasedimentary rocks to record maximum depositional ages of the protolith. The majority of the samples contain Mesozoic zircons—these likely correspond to metamorphosed equivalents of the Tipuma Formation, Mawi Complex, and Kembelangan Group. However, two samples yielded quite

the southern margin of the Philippine Sea Plate, which accreted to the northern margin of New Guinea (e.g., Ali & Hall, 1995; Hall, Ali, & Anderson, 1995; Hall, Ali, Anderson, & Baker, 1995).

### 5.5. Comparing our Results With Other Regional Data

The structural and geochronology results obtained in this study provide additional age data to be used to supplement tectonic interpretations of regional data sets. These new data indicate that there was a major change in the stress field in western New Guinea after ca. 5 Ma—an event that is recognized across other parts of New Guinea (e.g., Cloos et al., 2005) and eastern Indonesia (e.g., Hall, 1996, 2002). In the Wandamen Peninsula, this time marks a shift from the east–west crustal extension responsible for the formation of the Wandamen metamorphic core complex—to east–west transpression/shortening (with the earliest phase of this shortening also recording north–south ductile extension; Figures 13a–13c). This episode of transpression/shortening was recognized by Dow and Sukanto (1984) and Bailly et al. (2009). It is also recorded in

1. offshore seismic data which shows the Miocene Klasafet Formation (and age equivalent units) have been folded (e.g., Bailly et al., 2009, and arguably Pairault et al., 2003, as well as Sapin et al., 2009; Figure 3),
2. the local sea-level curve differs to global sea-level curves. The local sea-level curve shows a change from deeper water conditions (50–100 m) to shallower water conditions (0–10 m) between the Early to Late Pliocene (Gold, Burgess, et al., 2017; Gold, White, et al., 2017; Figure 12d),
3. the removal of early Pliocene to Mesozoic sequences due to erosion—as recorded in various hydrocarbon exploration wells (cf. Figure 18 in Gold, White, et al., 2017) as well as in regional offshore seismic imagery (e.g., Bailly et al., 2009; Pairault et al., 2003).

Our structural and geochronological data combined with these other data sources confirms the suggestion that the Lengguru Fold Belt must have developed due to a young (5–3 Ma) episode of crustal shortening (e.g., Decker et al., 2009; Dow et al., 1985; Moffat et al., 1991; Pieters et al., 1983; Visser & Hermes, 1962), rather than an earlier episode at ca. 11 Ma (e.g., Bailly et al., 2009; Francois et al., 2016).

The Wandamen region then went into a phase of crustal extension after ca. 3 Ma (Figure 13d). This phase of crustal extension is marked by the generation of brittle extensional faults observed in different parts of the Wandamen Peninsula (Figure 7), as well as in offshore seismic imagery of the Lengguru Fold Belt (e.g., Figure 3b; Bailly et al., 2009). The deformation history is also consistent with structures observed in seismic data within Cenderawasih Bay (e.g., Babault et al., 2018), yet there is no publicly available well data to provide age control on these structures. This extensional episode is also reflected by a phase of deeper water conditions in the local sea-level curve in the Pleistocene (Gold, White, et al., 2017) and coincides with the initiation of major strike-slip faults such as the Tarera-Aiduna Fault zones (e.g., Bailly et al., 2009; Pubellier & Ego, 2002). Aerial and satellite imagery also demonstrate that there is widespread evidence for relatively recent crustal extension throughout the Lengguru Fold Belt (Bailly et al., 2009; Pubellier & Ego, 2002)—these features are considered to have developed during the Quaternary–Recent and can likely be linked to the same processes responsible for the apparent extensional faulting observed along the eastern margin of the Wandamen Peninsula (Figure 7c).

### 5.6. Tectonic Mode Switches Over One to Two Million Years

Combining the structural and geochronological data obtained in this study, together with earlier work, shows that western New Guinea records multiple deformation episodes within a relatively short period of time. These structures could record reorientation of the stress field (e.g., Gray & Foster, 2004) or pulses of deformation associated with an episodically changing stress field (i.e., a tectonic mode switch; e.g., Lister & Forster, 2009). The data presented here indicate that the stress field episodically or progressively changed several times over the last six million years (Figure 13), indicating that episodes of crustal extension and crustal shortening can occur within periods of one to two million years. These findings further demonstrate that orogeny can be very short (e.g., Dewey, 2005) and that tectonic mode switches reported from older mountain belts are certainly possible within <10 million-year periods (e.g., Beltrando et al., 2008; Lister et al., 2001).

## 6. Conclusions

Structural observations indicate that the Wandamen Peninsula records multiple phases of metamorphism and deformation that we interpret to reflect several tectonic mode switches. New U-Pb and (U-Th)/He data obtained from two to three samples indicate that the tectono-thermal events occurred within the last six million years. An early phase of crustal extension occurred between ca. 6 and 5 Ma. These rocks were later overprinted by a phase of shortening that produced at least two generations of folds between 5 and 3 Ma. All of these fabrics were later cross-cut by brittle extensional faults (and minor thrusts) between 3 Ma and the present day, with uplift occurring progressively from north to south. We consider that the cross-cutting structures reflect several tectonic mode switches caused by changes in the stress field at the boundary between the Australian and Pacific Plates. The work presented here shows that tectonic mode switches can occur within one to two million-year periods. Such results should be considered in studies of older orogenic belts where it is more difficult to obtain precise dates for tectonic events.

## Acknowledgments

This work was largely funded by a consortium of oil exploration companies that sponsored the Southeast Asia Research Group at Royal Holloway University of London where L.T.W. was based as a Postdoctoral Research Fellow prior to moving to the University of Wollongong at the beginning of 2017. Additional funding was provided to L.T.W. from the GeoQuEST Research Centre at the University of Wollongong. Niko Asia and Repsol are also thanked for sponsoring the 2013 field campaign of L.T.W. The University of Melbourne Thermochronology Laboratory receives infrastructure support under the AuScope program of the National Collaborative Research Infrastructure Strategy (NCRIS). We thank Manuel Pubellier, Nuretdin Kaymakci, and an anonymous reviewer for thoughtful reviews. The work presented here also benefited from discussions with John Decker, Phil Teas, Angus Fergusson, Farid Ferdian, Benjamin Jost, Max Webb, David Gold, Manuel Gonzalez-Quijano, and Carlos Diaz. We thank Martin Rittner for the support when collecting LA-ICP-MS data as well as Kevin D'Souza for photographing several samples. The authors declare that there are no financial conflicts of interest associated with the publication of this work. Data supporting the conclusions can be obtained in the supporting information. Sample information has been catalogued using the international sample numbering scheme (ISDN) and managed within the SESAR database.

## References

- Aitchison, J. C., Ali, J. R., & Davis, A. M. (2007). When and where did India and Asia collide? *Journal of Geophysical Research*, 112, B05423. <https://doi.org/10.1029/2006JB004706>
- Ali, J. R., & Hall, R. (1995). Evolution of the boundary between the Philippine Sea Plate and Australia: Palaeomagnetic evidence from eastern Indonesia. *Tectonophysics*, 251, 251–275. [https://doi.org/10.1016/0040-1951\(95\)00029-1](https://doi.org/10.1016/0040-1951(95)00029-1)
- Babault, J., Viaplana-Muzas, M., Legrand, X., Van Den Driessche, J., Gonzalez-Quijano, M., & Mudd, S. M. (2018). Source-to-sink constraints on tectonic and sedimentary evolution of the western Central Range and Cenderawasih Bay (Indonesia). *Journal of Asian Earth Sciences*, 156, 265–287. <https://doi.org/10.1016/j.jseas.2018.02.004>
- Bailly, V., Pubellier, M., Ringenbach, J. C., de Sigoyer, J., & Sapin, F. (2009). Deformation zone “jumps” in a young convergent setting: the Lengguru fold-and-thrust belt, New Guinea Island. *Lithos*, 113(1–2), 306–317. <https://doi.org/10.1016/j.lithos.2009.08.013>
- Balanyá, J. C., García-Dueñas, V., Azañón, J. M., & Sánchez-Gómez, M. (1997). Alternating contractional and extensional events in the Alpujarride nappes of the Alboran Domain (Betics, Gibraltar Arc). *Tectonics*, 16, 226–238. <https://doi.org/10.1029/96TC03871>
- Baldwin, S. L., Fitzgerald, P. G., & Webb, L. E. (2012). Tectonics of the New Guinea region. *Annual Review of Earth and Planetary Sciences*, 40(1), 495–520. <https://doi.org/10.1146/annurev-earth-040809-152540>
- Beltrando, M., Hermann, J., Lister, G., & Compagnoni, R. (2007). On the evolution of orogens: Pressure cycles and deformation mode switches. *Earth and Planetary Science Letters*, 256(3–4), 372–388. <https://doi.org/10.1016/j.epsl.2007.01.022>
- Beltrando, M., Lister, G., Hermann, J., Forster, M., & Compagnoni, R. (2008). Deformation mode switches in the Penninic units of the Urtier Valley (Western Alps): Evidence for a dynamic orogen. *Journal of Structural Geology*, 30(2), 194–219. <https://doi.org/10.1016/j.jsg.2007.10.008>
- Black, L., Kamo, S., Allen, C., Davis, D., Aleinikoff, J., Valley, J., et al. (2004). Improved 206Pb/238U microprobe geochronology by the monitoring of a trace-element-related matrix effect; SHRIMP, ID-TIMS, ELA-ICP-MS and oxygen isotope documentation for a series of zircon standards. *Chemical Geology*, 205(1–2), 115–140. <https://doi.org/10.1016/j.chemgeo.2004.01.003>
- Bladon, G. M. (1988). Catalogue, appraisal, and significance of K-Ar isotopic ages determined for igneous and metamorphic rocks in Irian Jaya, 1–93.
- Brash, R. A., Henage, L. F., Harahap, B. H., Moffat, D. T., & Tauer, R. W. (1991). Stratigraphy and depositional history of the New Guinea Limestone Group, Lengguru, Irian Jaya. *Proceedings, Indonesian Petroleum Association*, 67–84.
- Charlton, T. R. (2010). The Pliocene-Recent anticlockwise rotation of the Bird's Head, the opening of the Aru Trough—Cenderawasih sphenochasm, and the closure of the Banda double arc. *Proceedings, Indonesian Petroleum Association*, 34<sup>th</sup> Annual Convention (IPA10-G-008), pp. 18.
- Cloos, M., Sapiie, B., Quarles van Ufford, A., Weiland, R. J., Warren, P. Q., & McMahon, T. P. (2005). Collisional delamination in New Guinea: The geotectonics of subducting slab breakoff. *Geological Society of America Special Papers*, 400, 51. <https://doi.org/10.1130/2005.2400>
- Collins, W. J. (2002). Hot orogens, tectonic switching, and creation of continental crust. *Geology*, 30(6), 535–538. [https://doi.org/10.1130/0091-7613\(2002\)030<0535:HOTSAC>2.0.CO;2](https://doi.org/10.1130/0091-7613(2002)030<0535:HOTSAC>2.0.CO;2)
- Davies, H. L. (2012). The geology of New Guinea—The cordilleran margin of the Australian continent. *Episodes*, 35(1), 87–102.
- Decker, J., Bergman, S. C., Teas, P. A., Baillie, P., & Orange, D. L. (2009). Constraints on the tectonic evolution of the Bird's Head, West Papua. *Proceedings, Indonesian Petroleum Association*, 33rd Annual Convention (IPA099-G-139), 25pp.
- Decker, J., Ferdian, F., Morton, A., Fanning, M., & White, L. T. (2017). New geochronology data from eastern Indonesia –An aid to understanding sedimentary provenance in a frontier region. *Proceedings, Indonesian Petroleum Association*, 41st Annual Convention (IPA17-551-G), 18 pp.
- Dewey, J. F. (2005). Orogeny can be very short. *Proceedings of the National Academy of Sciences of the United States of America*, 102(43), 15,286–15,293. <https://doi.org/10.1073/pnas.0505516102>
- Dow, D. B., & Ratman, N. (1981). Neogene tectonism, metamorphism, and magmatism in Western Irian Jaya, Indonesia. *Geosea Regional Conference*, Manila, 29–35.
- Dow, D. B., Robinson, G. P., Hartono, U., & Ratman, N. (1988). Geology of Irian Jaya, BMR-GRDC Preliminary Geological Report, 1–359.
- Dow, D. B., Robinson, G. P., & Ratman, N. (1985). New hypothesis for formation of Lengguru foldbelt, Irian Jaya, Indonesia. *AAPG Bulletin*, 69(2), 203–214.
- Dow, D. B., & Sukanto, R. (1984). Western Irian Jaya: The end-product of oblique plate convergence in the Late Tertiary. *Tectonophysics*, 106, 109–139. [https://doi.org/10.1016/0040-1951\(84\)90224-5](https://doi.org/10.1016/0040-1951(84)90224-5)
- Forster, M. A., & Lister, G. (2008). Tectonic sequence diagrams and the structural evolution of schists and gneisses in multiply deformed terranes. *Journal of the Geological Society*, 165(5), 923–939. <https://doi.org/10.1144/0016-76492007-016>
- Forster, M. A., & Lister, G. S. (2005). Several distinct tectono-metamorphic slices in the Cycladic eclogite-blueschist belt, Greece. *Contributions to Mineralogy and Petrology*, 150(5), 523–545. <https://doi.org/10.1007/s00410-005-0032-9>



- Fossen, H., & Tikoff, B. (1998). Extended models of transpression and transtension, and application to tectonic settings. In R. E. Holdsworth, R. A. Strachan, & J. F. Dewey (Eds.), *Continental transpressional and transtensional tectonics, Special Publications* (Vol. 135, pp. 15–33). London: Geological Society. <https://doi.org/10.1144/GSL.SP.1998.135.01.02>
- Fossen, H., Tikoff, B., & Teyssier, C. (1994). Strain modeling of transpressional and transtensional deformation. *Norsk Geologisk Tidsskrift*, 74, 134–145.
- Francois, C., De Sigoyer, J., Pubellier, M., Bailly, V., Cocherie, A., & Ringenbach, J.-C. (2016). Short-lived subduction and exhumation in Western Papua (Wandamen peninsula): Co-existence of HP and HT metamorphic rocks in a young geodynamic setting. *Lithos*, 266–267, 44–63. <https://doi.org/10.1016/j.lithos.2016.09.030>
- Froitzheim, N. (1992). Formation of recumbent folds during synorogenic crustal extension (Austroalpine nappes, Switzerland). *Geology*, 20, 923–926.
- Froitzheim, N., Schmid, S. M., & Conti, P. (1994). Repeated change from crustal shortening to orogen-parallel extension in the Austroalpine units of Graubünden. *Eclogae Geologicae Helveticae*, 87(2), 559–612. <https://doi.org/10.5169/seals-167471>
- Gleadow, A., Harrison, M., Kohn, B., Lugo-Zazueta, R., & Phillips, D. (2015). The Fish Canyon Tuff: A new look at an old low-temperature thermochronology standard. *Earth and Planetary Science Letters*, 424(C), 95–108. <https://doi.org/10.1016/j.epsl.2015.05.003>
- Gold, D. P., Burgess, P. M., & BouDagher-Fadel, M. K. (2017). Carbonate drowning successions of the Bird's Head, Indonesia. *Facies*, 63, 25. <https://doi.org/10.1007/s10347-017-0596-z>
- Gold, D. P., White, L. T., Gunawan, I., & Boudagher-Fadel, M. K. (2017). Relative sea-level change in western New Guinea recorded by regional biostratigraphic data. *Marine and Petroleum Geology*, 86, 1133–1158. <https://doi.org/10.1016/j.marpetgeo.2017.07.016>
- Gradstein, F. M., Ogg, J. G., Schmitz, M. D., & Ogg, G. M. (2012). *The geological time scale 2012* (1st ed.). Amsterdam; Boston: Elsevier.
- Gray, D. R., & Foster, D. A. (2004). <sup>40</sup>Ar/<sup>39</sup>Ar thermochronologic constraints on deformation, metamorphism and cooling/exhumation of a Mesozoic accretionary wedge, Otago Schist, New Zealand. *Tectonophysics*, 385, 181–210. <https://doi.org/10.1016/j.tecto.2004.05.001>
- Gunawan, I., Hall, R., & Sevastjanova, I. (2012). Age, character and provenance of the Tipuma Formation, West Papua: New Insights from detrital zircon dating. *Proceedings, Indonesian Petroleum Association*, 36, 1–14.
- Hall, R. (1996). Reconstructing Cenozoic SE Asia. In R. Hall & D. Blundell (Eds.), *Tectonic Evolution of Southeast Asia, Geological Society Special Publication 106*, 153–184. <https://doi.org/10.1144/GSL.SP.1996.106.01.11>
- Hall, R. (2002). Cenozoic geological and plate tectonic evolution of SE Asia and the SW Pacific: Computer-based reconstructions, model and animations. *Journal of Asian Earth Sciences*, 20, 353–431. [https://doi.org/10.1016/S1367-9120\(01\)00069-4](https://doi.org/10.1016/S1367-9120(01)00069-4)
- Hall, R. (2012). Late Jurassic–Cenozoic reconstructions of the Indonesian region and the Indian Ocean. *Tectonophysics*, 570–571, 1–41.
- Hall, R., Ali, J. R., & Anderson, C. D. (1995). Cenozoic motion of the Philippine Sea Plate: Paleomagnetic evidence from eastern Indonesia. *Tectonics*, 14, 1117–1132. <https://doi.org/10.1029/95TC01694>
- Hall, R., Ali, J. R., Anderson, C. D., & Baker, S. J. (1995). Origin and motion history of the Philippine Sea Plate. *Tectonophysics*, 251, 229–250. [https://doi.org/10.1016/0040-1951\(95\)00038-0](https://doi.org/10.1016/0040-1951(95)00038-0)
- Hennig, J., Hall, R., Forster, M. A., Kohn, B. P., & Lister, G. S. (2017). Rapid cooling and exhumation as a consequence of extension and crustal thinning: Inferences from the Late Miocene to Pliocene Palu Metamorphic Complex, Sulawesi, Indonesia. *Tectonophysics*, 712–713, 600–622.
- Hiess, J., Condon, D. J., & McLean, N. (2012). 238U/235U systematics in terrestrial uranium-bearing minerals. *Science*, 335(6076), 1610–1614. <https://doi.org/10.1126/science.1215507>
- Hill, K. C., & Hall, R. (2003). Mesozoic–Cenozoic evolution of Australia's New Guinea margin in a west Pacific context. *Geological Society of America Special Papers*, 372, 265–290.
- Holm, R. J., Rosenbaum, G., & Richards, S. W. (2016). Post 8Ma reconstruction of Papua New Guinea and Solomon Islands: Microplate tectonics in a convergent plate boundary setting. *Earth Science Reviews*, 156, 66–81. <https://doi.org/10.1016/j.earscirev.2016.03.005>
- Holm, R. J., Spandler, C., & Richards, S. W. (2013). Melanesian arc far-field response to collision of the Ontong Java Plateau: Geochronology and petrogenesis of the Simuku Igneous Complex, New Britain, Papua New Guinea. *Tectonophysics*, 603, 189–212. <https://doi.org/10.1016/j.tecto.2013.05.029>
- Holm, R. J., Spandler, C., & Richards, S. W. (2015). Continental collision, orogenesis and arc magmatism of the Miocene Maramuni arc, Papua New Guinea. *Gondwana Research*, 28, 1117–1136. <https://doi.org/10.1016/j.gr.2014.09.011>
- Horstwood, M. S. A., Köšler, J., Gehrels, G., Jackson, S. E., McLean, N. M., Paton, C., et al. (2016). Community-derived standards for LA-ICP-MS U-(Th)-Pb geochronology—Uncertainty propagation, age interpretation and data reporting. *Geostandards and Geoanalytical Research*, 40(3), 311–332. <https://doi.org/10.1111/j.1751-908X.2016.00379.x>
- Jost, B. J., Webb, M., & White, L. T. (2018). The Mesozoic and Palaeozoic granitoids of North-Western New Guinea. *Lithos* <https://doi.org/10.1016/j.lithos.2018.04.027>, 312–313, 223–243.
- Kohn, M. J., Corrie, S. L., & Markley, C. (2015). The fall and rise of metamorphic zircon. *American Mineralogist*, 100(4), 897–908. <https://doi.org/10.2138/am-2015-5064>
- Korchinski, M., Rey, P. F., Mondy, L., Teyssier, C., & Whitney, D. L. (2018). Numerical investigation of deep-crust behavior under lithospheric extension. *Tectonophysics*, 726, 137–146. <https://doi.org/10.1016/j.tecto.2017.12.029>
- Lister, G., & Forster, M. (2009). Tectonic mode switches and the nature of orogenesis. *Lithos*, 113(1–2), 274–291. <https://doi.org/10.1016/j.lithos.2008.10.024>
- Lister, G., Forster, M. A., & Rawling, T. J. (2001). Episodicity during orogenesis. *Geological Society of London, Special Publication*, 184(1), 89–113. <https://doi.org/10.1144/GSL.SP.2001.184.01.06>
- Moffat, D. T., Henage, L. F., Brash, R. A., Tauer, R. W., & Harahap, B. H. (1991). Lengguru, Irian Jaya: Prospect selection using field mapping, balanced cross-sections, and gravity modelling. *Proceedings, Indonesian Petroleum Association*, 1–22.
- Monnier, C., Girardeau, J., Pubellier, M., Polve, M., Permana, H., & Bellon, H. (1999). Petrology and geochemistry of the Cyclops ophiolites (Irian Jaya, East Indonesia): Consequences for the Cenozoic evolution of the north Australian margin. *Mineralogy and Petrology*, 65(1–2), 1–28. <https://doi.org/10.1007/BF01161574>
- Pairault, A. A., Hall, R., & Elders, C. F. (2003). Structural styles and tectonic evolution of the Seram Trough, Indonesia. *Marine and Petroleum Geology*, 20(10), 1141–1160. <https://doi.org/10.1016/j.marpetgeo.2003.10.001>
- Paton, C., Hellstrom, J., Paul, B., Woodhead, J., & Hergt, J. (2011). Lolite: Freeware for the visualisation and processing of mass spectrometric data. *Journal of Analytical Atomic Spectrometry*, 26(12), 2508–2511. <https://doi.org/10.1039/c1ja10172b>
- Paton, C., Woodhead, J. D., Hellstrom, J. C., Hergt, J. M., Greig, A., & Maas, R. (2010). Improved laser ablation U-Pb zircon geochronology through robust downhole fractionation correction. *Geochemistry, Geophysics, Geosystems*, 11, Q0AA06. <https://doi.org/10.1029/2009GC002618>

- Pearce, N. J. G., Perkins, W. T., Westgate, J. A., Gorton, M. P., Jackson, S. E., Neal, C. R., & Chenery, S. P. (1997). A compilation of new and published major and trace element data for NIST SRM 610 and NIST SRM 612 glass reference materials. *Geostandards Newsletter*, 21(1), 115–144. <https://doi.org/10.1111/j.1751-908X.1997.tb00538.x>
- Phillips, D., Matchan, E. L., Honda, M., & Kuiper, K. F. (2017). Astronomical calibration of  $^{40}\text{Ar}/^{39}\text{Ar}$  reference minerals using high-precision, multi-collector (ARGUS VI) mass spectrometry. *Geochimica et Cosmochimica Acta*, 196, 351–369. <https://doi.org/10.1016/j.gca.2016.09.027>
- Pieters, P. E., Pigram, C. J., Trail, D. S., Dow, D. B., Ratman, N., & Sukanto, R. (1983). The stratigraphy of western Irian Jaya. *Bulletin of the Geological Research and Development Centre*, 8, 14–48.
- Pigram, C. J., & Symonds, P. A. (1991). A review of the timing of the major tectonic events in the New Guinea Orogen. *Journal of Southeast Asian Earth Sciences*, 6(3–4), 307–318. [https://doi.org/10.1016/0743-9547\(91\)90076-A](https://doi.org/10.1016/0743-9547(91)90076-A)
- Pubellier, M., Ali, J., & Monnier, C. (2003). Cenozoic Plate interaction of the Australia and Philippine Sea Plates: “Hit-and-run” tectonics, 363(3–4), 181–199. [https://doi.org/10.1016/S0040-1951\(02\)00671-6](https://doi.org/10.1016/S0040-1951(02)00671-6)
- Pubellier, M., & Ego, F. (2002). Anatomy of an escape tectonic zone: Western Irian Jaya (Indonesia). *Tectonics*, 21(4), 1019. doi:<https://doi.org/10.1029/2001TC901038>
- Rawling, T. J., & Lister, G. S. (1999). Oscillating modes of orogeny in the southwest Pacific and the tectonic evolution of New Caledonia. *Geological Society Special Publication*, 154, 109–127. <https://doi.org/10.1144/GSL.SP.1999.154.01.05>
- Rey, P. F., Mondy, L., Duclaux, G., Teyssier, C., Whitney, D. L., Bocher, M., & Prigent, C. (2017). The origin of contractional structures in extensional gneiss domes. *Geology*, 45(3), 263–266. <https://doi.org/10.1130/G38595.1>
- Ridley, J. (1986). Parallel stretching lineations and fold axes oblique to a shear displacement direction—A model and observations. *Journal of Structural Geology*, 8(6), 647–653. [https://doi.org/10.1016/0191-8141\(86\)90070-2](https://doi.org/10.1016/0191-8141(86)90070-2)
- Robinson, G. P., Harahap, B. H., Suparman, M., & Bladon, G. M. (1990). Geology of the Fak Fak Sheet area, Irian Jaya, GRDC, 1–45.
- Robinson, G. P., Ryburn, R. J., Harahap, B. H., Tobing, S. L., Achdan, A., Bladon, G. M., & Pieters, P. E. (1990a). Geology of the Steenkool sheet area, Irian Jaya, GRDC, 1–45.
- Robinson, G. P., Ryburn, R. J., Harahap, B. H., Tobing, S. L., Bladon, G. M., & Pieters, P. E. (1990b). Geology of the Kaimana shear area, Irian Jaya, GRDC, 1–51.
- Sapin, F., Pubellier, M., Ringenbach, J.-C., & Bailly, V. (2009). Alternating thin versus thick-skinned decollements, example in a fast tectonic setting: The Misool–Onin–Kumawa Ridge (West Papua). *Journal of Structural Geology*, 31, 444–459. <https://doi.org/10.1016/j.jsg.2009.01.010>
- Schellart, W. P. (2017). A geodynamic model of subduction evolution and slab detachment to explain Australian plate acceleration and deceleration during the latest Cretaceous–early Cenozoic. *Lithosphere*, 9(6), 976–986. <https://doi.org/10.1130/L675.1>
- Schellart, W. P., & Spakman, W. (2015). Australian plate motion and topography linked to fossil New Guinea slab below Lake Eyre. *Earth and Planetary Science Letters*, 421(C), 107–116. <https://doi.org/10.1016/j.epsl.2015.03.036>
- Searle, M. P., Cooper, D., Rex, A. J., Herren, E., & Colchen, M. (1988). Collision tectonics of the Ladakh–Zaskar Himalaya [and discussion]. *Philosophical Transactions of the Royal Society of London. Series A. Mathematical and Physical Sciences*, 326, 117–150. <https://doi.org/10.1098/rsta.1988.0082>
- Sláma, J., Košler, J., Condon, D. J., Crowley, J. L., Gerdes, A., Hanchar, J. M., Horstwood, M. S. A., et al. (2008). Plešovice zircon—A new natural reference material for U–Pb and Hf isotopic microanalysis. *Chemical Geology*, 249(1–2), 1–35. <https://doi.org/10.1016/j.chemgeo.2007.11.005>
- Sutriyono, E., & Hill, K. C. (2001). Structure and hydrocarbon prospectivity of the Lengguru Fold Belt, Irian Jaya. *Proceedings, Indonesian Petroleum Association*, 28, 319–334.
- van den Ende, C., White, L. T., & van Welzen, P. C. (2017). The existence and break-up of the Antarctic land bridge as indicated by both amphipacific distributions and tectonics. *Gondwana Research*, 44(C), 219–227. <https://doi.org/10.1016/j.gr.2016.12.006>
- Vermesch, P. (2018). IsoplotR: A free and open toolbox for geochronology. *Geoscience Frontiers*, 9, 1479–1493. <https://doi.org/10.1016/j.gsf.2018.04.001>
- Viete, D. R., Oliver, G. J. H., Fraser, G. L., Forster, M. A., & Lister, G. S. (2013). Timing and heat sources for the Barrovian metamorphism, Scotland. *Lithos*, 177(C), 148–163. <https://doi.org/10.1016/j.lithos.2013.06.009>
- Viete, D. R., Richards, S. W., Lister, G. S., Oliver, G. J. H., & Banks, G. J. (2010). Lithospheric-scale extension during Grampian orogenesis in Scotland. *Geological Society of London, Special Publication*, 335(1), 121–160. <https://doi.org/10.1144/SP335.7>
- Visser, W. A., & Hermes, J. J. (1962). Geological results of the exploration for oil in Netherlands New Guinea, Geologische serie.
- Webb, M., & White, L. T. (2016). Age and nature of Triassic magmatism in the Netoni Intrusive Complex, West Papua, Indonesia. *Journal of Asian Earth Sciences*, 132, 58–74. <https://doi.org/10.1016/j.jseas.2016.09.019>
- White, L. T., Gibson, G. M., & Lister, G. S. (2013). A reassessment of paleogeographic reconstructions of eastern Gondwana: Bringing geology back into the equation. *Gondwana Research*, 24(3–4), 984–998. <https://doi.org/10.1016/j.gr.2013.06.009>
- Whitney, D. L., Teyssier, C., Rey, P., & Buck, W. R. (2013). Continental and oceanic core complexes. *Geological Society of America Bulletin*, 125, 273–298. <https://doi.org/10.1130/B30754.1>